Observations and modeling of air quality trends over 1990-2010 across the northern hemisphere: China, the United States and Europe

Jia Xing[1], Rohit Mathur[1], Jonathan Pleim[1], Christian Hogrefe[1], Chuen-Meei Gan[1], David C. Wong[1], Chao Wei[1, 2], Robert Gilliam[1], George Pouliot[1]

[1] The U.S. Environmental Protection Agency, Research Triangle Park, NC 27711, Durham, USA

[2] Multiphase Chemistry Department, Max Planck Institute for Chemistry, 55128 Mainz, Germany

Correspondence to: Jia Xing (xing.jia@epa.gov, xingjia@tsinghua.org.cn)

Abstract

Trends in air quality across the northern hemisphere over a 21-year period (1990-2010) were simulated using the CMAQ multiscale chemical transport model driven by meteorology from WRF simulations and internally consistent historical emission inventories obtained from EDGAR. Thorough comparison with several ground observation networks mostly over Europe and North America was conducted to evaluate the model performance as well as the ability of CMAQ to reproduce the observed trends in air quality over the past two decades in three regions: eastern China, the continental United States and Europe.

The model successfully reproduced the observed decreasing trends in SO_2, NO_2, maxima 8h O_3, SO_4^{2-} and EC in the U.S. and Europe. However, the model fails to reproduce the decreasing trends in NO_3^- in the US, potentially pointing to uncertainties of NH_3 emissions. The model failed to capture the 6-year trends of SO_2 and NO_2 in CN-API from 2005-2010, but reproduced the observed pattern of O_3 trends shown in three WDCGG sites over eastern Asia. Due to the coarse spatial resolution employed in these calculations, predicted SO_2 and NO_2 concentrations are underestimated relative to all urban networks, i.e., US-AQS (NMB=-38% and

-48%), EU-AIRBASE (NMB=-18% and -54%) and CN-API (NMB=-36% and -68%). Conversely, at the rural network EU-EMEP SO_2 is overestimated (NMB from 4% to 150%) while NO_2 is simulated well (NMB within ±15%) in all seasons. Correlations between simulated and observed winter time daily maxima 8-hr (DM8) O_3 are poor compared to other seasons for all networks. Better correlation between simulated and observed SO_4^{2-} was found compared to that for SO_2. Underestimation of summer SO_4^{2-} in the US may be associated with the uncertainty in precipitation and associated wet scavenging representation in the model. The model exhibits worse performance for NO_3^- predictions, particularly in summer, due to high uncertainties in the gas/particle partitioning of NO_3^- as well as seasonal variations of NH_3 emissions. There are high correlations ($R>0.5$) between observed and simulated EC, although the model underestimates the EC concentration by 65% due to the coarse grid resolution as well as uncertainties in the PM speciation profile associated with EC emissions.

The almost linear response seen in the trajectory of modeled O_3 changes in the eastern China over the past two decades, suggests that control strategies that focus on combined control of NO_x and VOC emissions with a ratio of 0.46 may provide the most effective means for O_3 reductions for the region devoid of non-linear response potentially associated with NO_x or VOC limitation resulting from alternate strategies. The response of O_3 is more sensitive to changes in NO_x emissions in the eastern U.S because the relative abundance of biogenic VOC emissions tends to reduce the effectiveness of VOC controls. Increasing NH_3 levels offset the relative effectiveness of NO_x controls in reducing the relative fraction of aerosol NO_3^- formed from declining NO_x emissions in the eastern U.S., while the control effectiveness was assured by the simultaneous control of NH_3 emission in Europe.

Keywords: Trends, CMAQ, modeling, air quality, sulfate, nitrate, ozone, northern hemisphere

1. Introduction

The last two decades have witnessed significant changes in air pollutant emissions across the globe. Developed countries in North America and Europe have implemented emission reduction measures which have led to a continuous improvement in air quality. Conversely, in developing regions of the world, in Asia in particular, though control actions have been taken, their effectiveness has been overwhelmed by the sharp increase in emissions resulting from increased energy demand associated with rapidly growing economies and populations. The striking contrast in the trends in air quality between developed and developing countries has been well discussed in recent years (e.g., Richter et al, 2005). It is also believed that the observed "dimming" and "brightening" trends over the past two decades is primarily related to the changes of emission patterns over northern hemisphere (e.g., Wild, 2009; Gan et al, 2014). Therefore, an accurate description of the decadal variations in emissions and associated aerosol burden in the atmosphere is the basis of any attempts to explain the causes of decadal changes in surface solar radiations and short-term climate forcing issues arising from human activities.

Improving air quality and protecting the health and welfare of their people is an important goal for any country. Studies on historical trends in air quality can provide an indication of progress in the direction as well as an assessment of future steps towards the goal. On the basis of long-term records, the effectiveness of past or current control policy can be evaluated and suitable control strategies can be designed for the future. In Europe and North America, several monitoring networks have been in operation for decades and observational records available at some networks are long enough to be used in trends analysis studies (e.g., Sickles and Shadwick (2007)). Such records are vital not only because they reflect the changes in air quality over time, but also because they can be used to evaluate long-term trends in air quality arising from

estimated changes in historical emissions, simulated by air quality models. Colette et al (2011) analyzed the air quality trends during 1998-2007 over Europe by using observations of European Monitoring and Evaluation Programme (EU-EMEP, http://www.emep.int) and the European Air quality data Base (EU-AIRBASE, http://acm.eionet.europa.eu/databases/airbase/) records as well as model simulations. Hogrefe et al (2009) adjusted six-year model simulations (2000-2005) by using the observed $PM_{2.5}$ species concentrations from the observations of Interagency Monitoring of Protected Visual Environments (US-IMPROVE, http://vista.cira.colostate.edu/improve/) and Chemical Speciation Network (CSN) sites in the northeastern US. Trends in O_3 concentration and SO_4^{2-}, NO_3^- depositions from 1988-2005 simulated by the same model were also compared with long term observations (Civerolo et al, 2010; Hogrefe et al, 2011). However, due to the large computational cost, very few studies have examined in decadal trend in air pollution over large regions such as northern hemisphere. Koumoutsaris and Bey (2012) evaluated the global model performance of O_3 trends simulation (1991–2005) through comparison with long-term observed records from EMEP, the World Data Centre for Greenhouse Gases (WDCGG, http://ds.data.jma.go.jp/gmd/wdcgg/) and the Clean Air Status and Trends Network (US- CASTNET, http://epa.gov/castnet/). Long-term records of lower troposphere O_3 concentrations from selected sites which are believed to represent baseline conditions in Europe (Logan et al., 2012) and the U.S. (Parrish et al., 2009; 2012) were used to make quantitative comparisons of simulation results from three chemistry-climate models (NCAR CAM-chem, GFDL-CM3, and GISS-E2-R) (Parrish et al., 2014). To date however limited attempts have been made to systematically assess long-term trends in multiple linked atmospheric pollutants (oxidants, particles and acidifying substances) across regional to hemispheric scales.

As a regional chemistry transport model (CTM), the Community Multiscale Air Quality (CMAQ) modeling (version 5.0) system (Binkowski and Roselle, 2003; Byun and Schere, 2006; Foley et al., 2010) has previously been successfully applied for several quality studies over North America (Eder and Yu, 2006; Appel et al, 2007, 2008; Mathur et al., 2008), Europe (Matthias et al., 2012; Kukkonen et al., 2012) and eastern Asia (Yamaji et al., 2006; Wang et al., 2011a; Xing et al., 2011a). However, the need for time varying lateral boundary conditions (LBCs) which are usually derived from global CTMs simulations limits its applications in trend analysis over decades. Recently, the applicability of CMAQ model has been successfully extended to hemispheric scales (Mathur et al., 2012; 2014), so that the application of hemispheric CMAQ provides a consistent approach to generate LBCs for nested regional domains employing finer resolution.

Changing emission patterns across the globe over the past two decades have influenced background air pollution levels for different regions across the northern hemisphere. To examine air quality trends in different regions over northern hemisphere, we used a multiscale chemical transport model (i.e., CMAQ) driven by historical emission inventories and meteorological dataset to simulate air quality from 1990-2010. The ability of the multiscale model to reproduce observed trends over the northern hemisphere, including North America, Europe and East Asia, was assessed. A brief description of the model configuration, emission processing and observations is given in section 2. The evaluation of model performance through comparison with long-term observation records is presented in section 3.1. The trends in both observed and simulated air quality are provided in section 3.2 and further discussed in section 4.

2. Method

2.1 Model configuration

Unlike the traditional regional studies with CMAQ, this study used a simulation domain extended to cover the entire northern hemisphere with a grid of 108 km×108 km resolution and 44 vertical layers of variable thickness between the surface and 50mb (Mathur et al., 2012; 2014). We selected three sub-regions, i.e., eastern China (20N-40N, 100E-125E), eastern US (28N-50N, 100W-70W) and Europe (35N-65N, 10W-30E), for further analysis and comparison with measurements. These three sub-regions are parts of the original northern hemispheric domain and no nested simulations were conducted.

The meteorological inputs for 21-year WRF simulations were derived from the NCEP/NCAR Reanalysis data which has 2.5 degree spatial, and 6-hour temporal resolution. NCEP ADP Operational Global Surface Observations were used for surface reanalysis which is used for indirect soil moisture and temperature nudging (Pleim and Xiu, 2003; Pleim and Gilliam, 2009) in the Pleim-Xiu Land Surface Model (PX LSM) (Pleim and Xiu 1995; Xiu and Pleim 2001). The WRF configurations also used MODIS land-use types with 20 categories, RRTMg shortwave and longwave radiation scheme (Iacono et al., 2008), and the ACM2 PBL model (Pleim 2007a, b). WRF performance for the simulation of hourly surface temperature (T), relative humidity, wind speed and direction was evaluated through comparison with observations from NOAA's National Climatic Data Center (NCDC) Integrated Surface Data (ISD with lite-format) which provides hourly (or with 3-hour interval) meteorological observations over a long historical period across the globe. The mean bias of T, wind-speed and direction over the simulation domain is -0.4 K, 0.4 m s^{-1} and -3 degree respectively, within the benchmark range suggested by Emery et al. (2001) for retrospective regional-scale model applications which is ⩽

$\pm$0.5 K, $\leqslant \pm$0.5 m s^{-1} and $\leqslant \pm$10 degree respectively.

2.2 Emission inventories from 1990-2010

Fig. 1 presents a flow chart of the approach to emission processing employed in creating model inputs spanning the 21-year period. EDGAR (Emission Database for Global Atmospheric Research, version 4.2) (European Commission, 2011) provides a consistent global emission inventories for 1970-2008 for 17 anthropogenic sectors on a 0.1°×0.1° resolution. In this study, we used year specific EDGAR emission for the period 1990-2008. Estimates for 2009 and 2010 were derived from projections based on three most recent references for the United States (Xing et al, 2013), Europe (EEA, 2012) and China (He, 2012). In Europe and North America, pollutant emissions, SO_2 and NO_x in particular, have seen continuous reductions during 1990-2010 (refer to Fig. 2). In contrast, NO_x and VOC emissions in China have continuously increased, while SO_2 increased during 1990-2006 then decreased from 2007 to 2010 due to more recent strict controls (Zhao et al., 2013; Wang et al., 2014). Emissions in other areas during 2009-2010 were kept the same as the 2008 values. Additionally, since EDGARv4.2 provides only PM_{10} emissions, $PM_{2.5}$ emissions were estimated by deriving the ratio of $PM_{2.5}$ to PM_{10} from the 2000-2005 EDGAR HTAP (Hemispheric Transport of Air Pollution, version 1) inventory (Janssens-Maenhout et al, 2012) which provides both PM_{10} and $PM_{2.5}$ emissions and then applying this ratio to split EDGARv4.2 PM_{10} emissions into $PM_{2.5}$ and $PM_{2.5-10}$. Biogenic VOC and lightning NOx emissions were obtained from GEIA (Global Emission Inventory Activity) (Guenther et al., 1995; Price et al, 1997) and were kept the same for all years during 1990-2010. The 0.1° resolution gridded data was spatially allocated to the CMAQ grid ensuring conservation of mass. Vertical profiles for anthropogenic sectors and lightning were based on Simpson et al (2003) and Ott et al (2010), respectively. The annual mean emissions in each sector were distributed into each hour

for each simulated day using the EDGAR default temporal profiles which are primarily based on some western European data (http://themasites.pbl.nl/tridion/en/themasites/edgar/documentation/content/Temporal-variation.html). Emissions of $PM_{2.5}$ and NMVOC were further speciated into AERO6 and CB05 species based on default profiles in Sparse Matrix Operator Kernel Emissions modeling system (SMOKE, http://cmascenter.org/smoke/) which is primarily based on data for the United States. Uncertainties are expected when region specific temporal and speciation profiles are applied to all other counties; however this approach is reasonable given the lack of any additional information. Further improvement and data are needed to develop more representative profiles for other countries.

2.3 Observed long-term trends

Table 1 summarizes the dataset used in this study, which includes three networks in the United States, i.e., Air Quality System, (US-AQS, http://www.epa.gov/ttn/airs/airsaqs/), US-CASTNET and US-IMPROVE; two networks in Europe, i.e., EU-EMEP and EU-AIRBASE; one in China (CN-API, Air Pollution Index) and one global network (WDCGG). Among these, records of US-CASTNET, US-IMPROVE and EU-EMEP are specifically designed for trend assessments since most of their sites are located in rural background areas to represent regional atmospheric pollution. Sites in US-AQS and EU-AIRBASE are typically closer to urban areas and may be impacted by local pollution and features sub-grid to the model resolution, thus are representative of much smaller regions. To obtain a more valid analysis, the US-AQS and EU-AIRBASE data were averaged over the 108 km grid cells before comparing with the model. CN-API is the average of observed air pollutant concentrations from urban monitoring sites in each city and represents records in 7 Chinese cities (i.e., Beijing, Shanghai, Guangzhou, Xi'an, Wuhan,

Guiyang, Guilin which are located in north China plain, Yangtze-river delta, Pearl-river delta, northwest China, central China and south China respectively) where long-term observations are available starting from 2005. (Jiang et al, 2004; Wang et al, 2011a). In addition, 3 selected WDCGG sites were used for O_3 trends analysis in East Asia. Only data at sites that covered the 75% of entire 21-year period (i.e., at least 18 available years with >75% coverage for each year) is considered except in the case of CN-API which was only recently set up in early 2000s and in the case of US-CASTNET (for O_3 only) because most sites have no O_3 records in winter (criteria set as at least 15 available years with >75% coverage from March to November for each year). Details about the time-period covered, the number of sites selected for analysis as well as the record frequency for each network can be found in Table 1. Model results at each monitor location were matched in time to the available record; thus model data was not considered during periods of missing observations, in either the statistical evaluation or in the trend analysis.

To evaluate the model's performance, model-observed comparisons were conducted by network and pollutant. Five statistical measures: correlation coefficient (R), Mean Bias (MB), Normalized Mean Bias (NMB), Root Mean Squared Error (RMSE) and Normalized Mean Error (NME) are employed for evaluation. In consideration of the limited length of record, this study only focuses on linear trends (Colette et al, 2011). The linear least square fit method was employed and significance of trends was examined with a Student t-test at the 95% confidence level (p=0.05).

3. Result

3.1 Model performance

Table 2 summaries the statistics of model performance for gaseous species (Table 2a) and fine particles (Table 2b).

3.1.1 SO_2 and NO_2 concentration

Model performance characteristics for SO_2, primarily emitted from point sources, can largely be attributed to artificial dilution effects over the large grid volumes employed here. As expected, a hemispherical simulation with relatively coarse spatial resolution is unable to accurately capture the peak values. As seen in Table 2a, SO_2 is underestimated for all urban networks characterized by higher concentrations than rural network, i.e., US-AQS underestimated by 38%, EU-AIRBASE by 17% and CN-API by 36%. For rural network EU-EMEP, SO_2 is overestimated in all seasons (4-150%). A small bias is evident for US-CASTNET annual concentrations since the overestimation in fall is compensated by the underestimation in spring and winter.

Similar performance is noted for simulated NO_2. The model significantly underestimates NO_2 at urban networks: US-AQS by 48%, EU-AIRBASE by 54% and CN-API by 68%. However, much better performance is noted at sites in the rural network EU-EMEP with bias within ±15% in all seasons. Though the model-observation correlation coefficients (R) are low for EU-AIRBASE (0.4) and CN-API (0.08) on annual basis, the MB in EU-AIRBASE (-13.9 µg m^{-3}) is comparable with previous modeling as reported by Colette et al (2011) (-6.5 to -18.1 µg m^{-3}) and the magnitude of NMB in CN-API (67.5%) is comparable with Wang et al (2009) (-61.2 to -81.3%) but in opposite direction. It is expected that the performance should be better when simulations are conducted with finer horizontal resolution and with more accurate spatially-resolved emissions.

3.1.2 O_3 concentration

Model performance for O_3 is examined through comparisons of seasonal or annual maxima of the daily maxima 8-hr (DM8) average or 1-hour values since those are the metrics most

relevant to air quality standards and health assessments.

Correlation coefficients in EU-AIRBASE (0.4) are lower than Colette et al (2011) (0.6-0.8) because the frequency of the observed record used in this study is annual-, and therefore, the correlation coefficients calculated here do not benefit from the fact that the model simulations generally capture the observed seasonal cycle. However, the MB (14.4 µg m^{-3}) is comparable with that reported in Colette et al (2011) (-4.3 to 18.5µg m^{-3}). Simulations in winter (R=0.3-0.5) have the worst correlation with observations for all networks compared to those in other seasons (R=0.6-0.8). On the other hand, both NMB (-13.6 to 16.9%) and NME (< 25.9%) are fairly small in all seasons and comparable with that reported by Zhang et al. (2009) (NMB: -10.6 to 15.9%; NME: <25.4%) and Wang et al. (2009) (|NMB|<37.9 %).

3.1.3 SO_4^{2-}, NO_3^- and NH_4^+ concentration

SO_4^{2-} which is formed from the oxidation of SO_2, is the predominant inorganic aerosol component. In general, SO_4^{2-} concentrations show a strong positive response to the changes in SO_2 emissions (Butler and Lakens, 1991), though the SO_2 effective cloud oxidation rate can be affected by NH_3 (Pandis and Seinfeld, 1989; Tsimpidi et al., 2007). As a secondary species, SO_4^{2-} is widely spread over the region, unlike SO_2 which is usually more localized to source areas. As seen in Table 2b, correlation coefficients for SO_4^{2-} simulation (0.5-0.9) are higher than those for SO_2 (0.4-0.8). The NMBs for US-CASTNET (-8 to -45%) and US-IMPROVE (-29 to 22%) are comparable with the results reported by Zhang et al. (2009), which are -23 to 22% and -8 to 16%, Eder and Yu. (2006), which are -10% and -5% on annual level, and Wang et al. (2009) (|NMB|<55%). Significant SO_4^{2-} underestimation is noted during summer at both US-CASTNET (by 45.2%) and US-IMPROVE (by 28.9%). Some studies also found similar under-prediction in their simulations and they attributed such low biases to the uncertainty in precipitation and

overestimation of wet-scavenging. However, precipitation simulated in this study is underestimated domain-wide by 4% (in summer) to 65% (in winter). Wang et al (2009) found similar underestimation of precipitation from -31% to -41%, but SO_4^{2-} was over-predicted because higher SO_2 emissions were used. Future investigation of the low bias in predicted SO_4^{2-} is still necessary. Better performance is shown at EU-EMEP, with NMB within ±30%. The difference in sulfate biases between the U.S. networks and the European network might be associated with the different SO_2 biases, i.e., a moderate bias (NMB=-9.4%) in US-CASTNET but a relatively larger bias (NMB=+67%) in EU-EMEP. The transition rate from SO_2 to SO_4^{2-} is likely underestimated in both regions, leading to the underestimation of SO_4^{2-} in the U.S. and the better estimates of SO_4^{2-} in Europe.

Worse performance for NO_3^- prediction is expected because of higher uncertainties in representing the gas/particle partitioning of airborne nitrate (Mathur and Dennis, 2003; Eder and Yu, 2006). Especially in summer when SO_4^{2-} concentrations are higher and available NH_3 preferentially react to form ammonium sulfate, leading to low ambient NO_3^- level. Simulated and observed NO_3^- have the lowest correlations for both US-CASTNET and US-IMPROVE sites (R=0.31 and 0.10 respectively) during summer compared those in other seasons (R=0.7). Similar magnitudes of NMB (-56 to 59%) and NME (89 to 197%) at US-IMPROVE sites were reported by Wang et al. (2009) and Zhang et al. (2009). The underestimation in summer and overestimation in spring / winter are found relative to both CASTNET (NMB: -48% and 93/75%) and IMPROVE (NMB: -41% and 107/95%) and comparable to previous CMAQ analysis of Eder and Yu (2006) ($|NMB| > 40\%$). Uncertainties in NH_3 emission particularly in the seasonal temporal profile may also contribute to such bias characteristics. Slightly better performance is noted for NO_3^- at EU-EMEP sites, with higher R (>0.6) and smaller bias (NMB: -67% to 23%)

for all seasons.

Performance for NH_4^+ simulation is better than that of NO_3^- but slightly worse than for SO_4^{2-}. The NMB for US-CASTNET is -54 to 23% which is comparable with Wang et al. (2009) (|NMB|<50%). Similar performance statistics are shown for EU-EMEP (NMB: -15 to 68%).

3.1.4 Elemental Carbon (EC) concentration

EC being a primary pollutant, its spatial distributions exhibit strong correlation to its emissions. The correlation between the observed and simulated EC concentrations is high with R >0.5, though the model significantly underestimates the concentrations. NMB up to −74% which is worse than previous modeling studies utilizing relatively higher spatial resolution (Zhang et al., 2009; NMB = −15.4 to 8 %; Eder and Yu, 2006; NMB = −6 %), but the magnitude of NMB is comparable with Wang et al. (2009) (NMB= 101.7%) which also utilized coarse spatial resolution. Some previous CMAQ modeling studies (Tesche et al., 2006; Appel et al., 2008) with higher spatial resolution also found the similar underestimation of EC, indicating other factors besides model resolution, such as uncertainties of PM speciation profiles used to estimate the EC emissions might also contribute to such low biases.

3.2 Trend analysis

Simulated trends in SO_2, NO_2, O_3, SO_4^{2-}, NO_3^-, NH_4^+ and EC concentrations in three regions (Eastern China, Eastern US and Europe) are given in Table 3. To help understand the changes, trends in input emissions used in this study are also provided in Table 3 as well as depicted in Fig. 2. Capability of the CMAQ model to capture the observed trends was examined through comparisons with network measurements, and both simulated and observed trends are quantified in Table 4 and Figures 3-9.

3.2.1 SO_2 and NO_2 trend

Simulated trends in both SO_2 and NO_2 concentrations over the northern hemisphere reflect trends in SO_2 and NO_x emissions, respectively (see Fig. 2a-b, Fig. 3a and Fig. 4a), with pronounced increasing trend in Asia and decreasing trend in Europe and North America. Particularly, in China annual change rates of SO_2 and NO_2 concentration are about 2.7% and 4.1% which are comparable to their corresponding emission rates (SO_2 and NO_x) of 3.2% and 4.3% respectively. Annual change rates of SO_2 / NO_2 concentrations in the US (-5.7% / -1.4%) and Europe (-5.1% / -1.2%) are also close to the rates of emission changes in both regions, at -5.4% / -1.8% and -5.4% / -1.5% respectively.

Such decreasing trends in the US and Europe are comparable with those inferred from observations at the different networks. The annual change rates of SO_2 observed from US-CASTNET and US-AQS are -5.0% and -5.3%, close to that simulated by the model as -6.6% and -6.5%. Most of the reductions are located in the eastern US as seen in Fig.3e-f. The model was unable to capture the increasing trend at two of the eastern AQS sites and also the large decreasing trend at a few sites in the mid-west. It should be noted that the AQS SO_2 measurements predominantly represent urban conditions, and the ability of a coarse resolution model in capturing SO_2 levels and trends is influenced both by its inability to accurately represent sub-grid variability as well as changes in local emissions. For instance, the monitor in Kansas City, MO shows sharp increase in SO_2 levels starting 2003; in contrast the grid averaged SO_2 emissions in the corresponding model cell show systematic decreasing trends over the 21-year period resulting in the simulated decreasing SO_2 trend at this location. Also, as seen in the scatter plots in these panels, the pathway of such reductions from 1990 to 2010 is in good agreement between observation and simulation. Stronger trends are noted in winter when SO_2 concentrations are higher compared to other seasons in both observed (-0.368 $\mu g\ m^{-3}\ yr^{-1}$) and

simulated trend (-0.366 μg m^{-3} yr^{-1}) at US-CASTNET (see Table 4). Annual change rates of SO_2 observed from EU-AIRBASE and EU-EMEP are -8.9% and -7.3% which are close to that simulated by the model at -5.9% and -6.1%, with higher rates in winter when SO_2 concentration are at their highest level. Significant reductions are found at locations in Southern UK, Benelux, Germany, Italy, Czech Republic, Poland, Hungary and Romania.

The overall reductions in NO_2 from 1990 to 2010 are also in good agreement between the observations and model simulations. Observed decreasing trends of NO_2 concentrations (and annual change rate) are shown in urban networks, i.e., US-AQS and EU-AIRBASE are -0.63 μg m^{-3} yr^{-1} (-2.3%) and -0.64μg m^{-3} yr^{-1} (-1.9%) respectively. Model simulated trends (and annual change rate) at these two urban network, -0.32 μg m^{-3} yr^{-1} (-2.2%) and -0.14 μg m^{-3} yr^{-1} (-0.9%) respectively, are however underestimated. The reason might be associated with the underestimation of NO_2 concentrations. The model slightly overestimated the trends (annual change rates as well) at the rural EU-EMEP network (-0.16 μg m^{-3} yr^{-1} (-2.0%) from the model, compared to the observed trends of -0.13 μg m^{-3} yr^{-1} (-1.7%)). Such decreasing trends are more pronounced over the eastern US and California as well as Southern UK, Northern France, Benelux and Germany.

Large increases in the remotely sensed NO_2 vertical column density (VCD) over eastern China over the past decade has been noted in many studies (Richter et al., 2005; Irie et al, 2005; Akimoto et al., 2006; Zhang et al., 2007) but very limited in-situ data is available. Trends in SO_2 and NO_2 inferred from available CN-API data (for 6 years) were not significant (Table 4 and Fig. 3-4b); the model was unable to capture these trends, yielding trends more similar to those of the emissions. These discrepancies could likely arise from uncertainties in local emissions as well as the coarse spatial resolution which limits the model's ability to represent pollution distribution at

finer scale which is likely captured at these monitors. Some industries were moved out from city center to rural area nearby so that the improvement of local air quality observed in city center cannot be captured by large scale simulations. However, the model results agree with the findings from studies analyzing satellite information over Asia. For example, Zhang et al. (2012) analyzed SCIAMACHY-SO_2 VCD during 2004-2009, suggesting a continuous increase in tropospheric SO_2 loading in West China, but transition from increase to decrease in 2007 in East China resulting from controls.

3.2.2 O_3 trends

Ozone concentrations are sensitive to the control of NO_x and VOC emissions and studies have indicated that control in NO_x emission without a simultaneous significant reduction of VOC might lead to an increase of daily O_3 due to the switch from VOC-limited to NO_x-limited regime (e.g., Chameides et al., 1992; Sillman, 1999). However, O_3 chemistry is likely to be at NO_x-limited regime during periods of heavy photochemical pollution (Trainer et al, 1993; Xing et al., 2011b), suggesting that NO_x controls are more effective in reducing annual maximum (rather than average) of DM8 O_3. Therefore, trends in NO_x emission are more likely to have positive correlation with trends in annual maximum (rather than average) of DM8 O_3. As expected, simulated trend of annual maximum of DM8 O_3 concentration (see Fig.5a) looks quite similar to the NO_x and VOC emission trends (Fig. 2b-c). The simulated annual increasing rate of annual maximum of DM8 O_3 in eastern China is 1.49%, which is associated with the increase in NO_x and VOC emissions (by 4.3% and 2.3% per year). In contrast, due to reductions of emissions, substantial decreasing trends in annual maximum of DM8 O_3 are apparent in both the eastern US and Europe, with magnitudes of -0.66% and -0.54% per year, respectively (see Table 3). Significant increases of O_3 are also shown in northern India, west-Asia and sub-Saharan Africa

where both NO_x and VOC emissions have increased during this period (see Fig.2b-c).

Observed decreasing trends in annual maximum of DM8 O_3 concentrations (and annual change rate) in EU- EMEP, EU-AIRBASE and US-CASTNET are -1.07 μg m^{-3} yr^{-1} (-0.7%), -1.35μg m^{-3} yr^{-1} (-0.8%) and -1.86 μg m^{-3} yr^{-1} (-1.1%) respectively. Similar trends are estimated by the model simulation for both networks, i.e., -1.31 μg m^{-3} yr^{-1} (-0.9%), -2.13μg m^{-3} yr^{-1} (-1.1%) and -0.95 μg m^{-3} yr^{-1} (-0.6%) (see Table 4). The failure to capture the slightly increasing trends in observations in the urban network (i.e., EU-AIRBASE) might be associated with the limitation by coarse spatial resolution that causes the model to fail to represent the VOC-limited regime at these urban locations and a likely switch of O_3 chemistry from VOC- to NO_x- limited regime which usually goes along with the transition from urban to rural area (e.g., Xing et al., 2011b). Such decreasing trends are noted in all seasons except during winter when O_3 is at the lowest level. In contrast, the most significant reduction occurred in summer when O_3 concentrations are at the highest. The spatial pattern of O_3 trends is quite similar to that of NO_2, with more pronounced decrease in regions downwind of urban areas across the eastern US and California as well as Southern UK, Northern France, Benelux and Germany. The reason for increasing trends shown in both observed and model in mid-west of US might be explained by the changes in local emissions (less or no controls in mid-west) as well as increasing long-range transport of pollutants across the Pacific (Mathur et al., 2014). Analysis of long-term observations at remote sites along the western U.S. (e.g., Jaffe and Ray, 2007; Parrish et al., 2009) also show increasing trends in O_3 within the boundary layer attributable to inflow to the western U.S. from the Pacific.

Though long-term observation records of O_3 are not available in China, recent studies have suggested increasing trends similar to those found here. For instance, Xu et al (2011) suggested

significant increasing trends in tropospheric ozone residual over the North China Plain. Ding et al (2008) suggest that O_3 in the lower troposphere over Beijing had a strong positive trend (2% per year) during the period 1995 to 2005. Ozonesonde measurements analyzed by Wang et al (2012) suggests a clear positive trend in the maximum summer ozone concentration (3.4% per year) over the Beijing area during 2002-2010. In this study, the trend in summer maximum of DM8 ozone concentration in Beijing during 1990 to 2010 is estimated to be 2% per year, which is comparable to that inferred from observations in these two recent studies.

Observation records at three sites in WDCGG network were used to investigate trends in O_3 distribution in eastern Asia. One of these sites, Minamitorishima (noted as S1, lat: 24.28N, lon: 153.98E), is located far from land and can be considered to be a representative of clean conditions, while two sites located on Honshu island, i.e., Tsukuba (noted as S2, lat: 36.05, lon: 140.13) which is to the northwest of Tokyo and closest to urban regions, and Ryori (noted as S3, lat: 39.03, lon: 141.82) which is in the north and representative of rural conditions. The model generally captured the observed pattern of O_3 trends at each site. For the clean site (S1), no significant trends are inferred either in the observed or the simulated maximum of DM8 O_3. However, for the urban site (S2), significant reduction, particularly during summer, is noted in the observed values and is reflective of emission reductions in Japan during past two decades (e.g., Wakamatsu et al., 2013). In contrast, increasing trends are inferred at the rural site (S3) in all seasons expect fall, presumably, representing transport from upwind locations in East Asia. The model produces similar magnitude (though smaller significance) of the decreasing/increasing trends at S2/S3. The contrasting trends at sites S2 and S3 likely result from different controls in local emissions as well as transboundary transport.

3.2.3 SO_4^{2-}, NO_3^- and NH_4^+ trends

Simulated SO_4^{2-} shows a pronounced increasing trend in eastern China (2.8% per year) and decrease in the US (-3.2% per year) and EUROPE (-3.7% per year) which is consistent with, though slightly smaller in magnitude, with trends in SO_2 emissions in these regions (see Table 3 and Fig. 6).

Simulated SO_4^{2-} trends are in a good agreement with observed trends inferred from all three networks. Simulated trends in SO_4^{2-} concentrations (and annual change rate) at US-CASTNET, US-IMPROVE and EU-EMEP are -0.09 μg m^{-3} yr^{-1} (-3.5%), -0.03 μg m^{-3} yr^{-1} (-2.1%) and -0.09 μg m^{-3} yr^{-1} (-3.6%), which is comparable with the observed trends of -0.10 μg m^{-3} yr^{-1} (-2.9%), -0.03 μg m^{-3} yr^{-1} (-2.4%) and -0.10 μg m^{-3} yr^{-1} (-4.1%), respectively. More significant trends are noted in summer compared to other seasons because of relatively higher summer time SO_4^{2-} concentrations. Average trends at US-CASTNET are more significant than those at IMPROVE because majority of CASTNET sites are located in the eastern US which witnessed stronger reductions in SO_2 emissions. In Europe, most SO_4^{2-} reductions are found in central to eastern Europe, i.e., Germany, Czech, Poland, Hungary, Benelux, Italy, and Romania.

NH_3 emission plays an important role in NO_3^- formation (Mathur and Dennis, 2003; Wang et al., 2011b). Growth in NH_3 emission or reduction in SO_2 emission (consequently more free NH_3 due to less association with SO_4^{2-}) without simultaneous reduction in NO_x emission can enhance NO_3^- concentration especially under NH_3 poor conditions (Pinder et al., 2008a; Blanchard et al., 2007). As illustrated in Fig. 7, growth in both NO_x and NH_3 emissions results in the increasing trend in airborne NO_3^- in China (5.4% per year), while reductions in emissions of both results in the decreasing trend in Europe (-1.8% per year). In contrast, over the past two decades in the US, a reduction in SO_2 and NO_x accompanied with a growth in NH_3 emission results in different trends across different seasons. The model fails to reproduce the decreasing

trend in NO_3^- at both US-CASTNET and US-IMPROVE in spring, summer and fall though the significance of the trend is small. However, both simulated and observed NO_3^- show an increasing trend in winter values when NO_3^- is at the highest level. Similar observed increasing trend is noted during winter at the EU-EMEP monitors, which is not captured by the model. The decreasing trend at the EU-EMEP locations during other seasons is however captured by the model. Successful reproduction of NO_3^- trends depends on an accurate baseline emission as well as an accurate representation of changes in historical NH_3 emission. Unfortunately, both current NH_3 emission and their historical trends over the globe still suffer from large uncertainties (e.g., Heald et al, 2012) and likely contribute to the significant bias in the simulated NO_3^- trend.

NH_4^+ is simulated based on the thermodynamic equilibrium between the NO_x-SO_x-NH_x species. It shows a similar increasing trend in China (3.4%) and a decreasing trend in the US (-0.7%) and Europe (-2.9%), as illustrated in Fig. 8. NH_4^+ simulation suffers the same uncertainties as NO_3^- which leads to difficulties in reproducing the trend in observations (see Table 4).

3.2.4 Elemental Carbon (EC) trends

Growth of human activities such as biomass burning and open fires results in the simulated increasing trends in EC levels in China (1.0%; see Table 3), India and sub-Saharan Africa (see Fig. 9). In contrast, continuous controls have led to a decreasing trend in EC concentrations in the US (-3.4%) and Europe (-2.5%). The observed trend in EC at US-IMPROVE, i.e., -0.006 μg m^{-3} yr^{-1} (-2.6%) is well reproduced by the model, i.e., -0.003 μg m^{-3} yr^{-1} (-3.3%). Both observations and the model suggest higher magnitudes of trends during fall and winter, and are likely associated with higher ambient levels during these seasons.

Decreasing trend of EC in Europe has also been observed in other studies (Järvi et al.,

2008). The model estimates a consistent decreasing EC trend in the Canadian Arctic (see Fig. 9) which is mainly impacted by emissions from Europe and Russia during winter and spring as demonstrated by Sharma et al (2004) who analyzed in-situ ground-level observations of aerosol black carbon between 1989 and 2002. The increasing trend of EC in southern Asia is corroborated by the evidence found from the Nam Co Lake (located in the central Tibetan Plateau) sediments indicating a recent rise in BC deposition flux (Cong et al., 2013).

4. Discussion

4.1 O_3 chemistry

As discussed in section 3.2.2, the response of O_3 concentration depends on changes in NO_x and VOC emissions, and the non-linear chemistry associated with the subsequent VOC- or NO_x-limited environment. The response of O_3 to changing levels of NO_x and VOC have previously been examined through a variety of methods ranging from isopleths created from chemistry box-model calculations to detailed spatially varying response surfaces developed from output of hundreds of simulations with detailed air pollution modeling systems (e.g., Xing et al., 2011b). Exploration of the changes in O_3 levels in response to historical (and geographically varying) changes in NO_x and VOC emissions, as captured by the multi-decadal simulations presented here, provide a unique opportunity to develop insights into factors controlling changes in O_3 production and distributions.

Fig. 10 attempts to summarize the changes in NO_x and VOC emissions as well as the surface O_3 response during the 1990-2010 period for the three regions; the figures in the left panel illustrate the changes in emissions relative to the 1990 values and the figures in the right panel show the corresponding percentage change in both the maximum and the average of the DM8 O_3 for each year. As can be noted, the relative changes in NO_x and VOC emissions vary

significantly over different time-period for different regions. Based on the emission estimates, simultaneous growth of VOC and NO_x emissions is noted in China with a ratio of 0.46 (i.e., x% NO_x growth along with 0.46x% VOC growth on a basis of 1990 emission level). The modeled increases in both maximum and average of DM8 O_3 values in China during this period are significant. The almost linear response seen in the trajectory of modeled O_3 changes in the region over the past two decades, suggests that control strategies that focus on combined control of NO_x and VOC emissions with a ratio of 0.46 may provide the most effective means for O_3 reductions for the region devoid of non-linear response potentially associated with NO_x or VOC limitation resulting from alternate strategies. The ratio suggested is less than 1 indicating greater sensitivity of ozone to NO_x emissions than VOC emissions. It's also obvious to see that the rate of O_3 increase was much smaller during 1995-2002 which was the period when VOC emission growth was much greater than that of NO_x emissions in China.

In contrast, trends in emissions over the eastern US indicate significant reduction in VOC emissions compared to NO_x prior to 2000. NO_x emission increased slightly during 1996-2000, and then decreased significantly resulting from regional control measures. Change of O_3 during the first decade (1990-2000) when VOC controls were dominant (reduction ratio of VOC and NO_x is -42% and -4% respectively) is smaller (-2%) than that in the subsequent decade (2000-2010) when NO_x controls were dominant (reduction ratio of VOC and NO_x is -13% and -33%, respectively) leading to an estimated reduction of -11% in ambient O_3. Additionally, model simulations also show an increase in O_3 during 1997-1999 when NO_x emissions were estimated to increase. Thus, the response of O_3 is more sensitive to changes in NO_x emissions in the eastern US. The relative abundance of biogenic VOC emissions that tend to reduce the effectiveness of VOC controls, contributes to this differing response.

In Europe, simultaneous control of NO_x and VOC with a ratio of 1.8 during 1990-2010 result in systematic reduction in ambient O_3 levels. Interestingly, the reductions in the annual maximum of the regionally-averaged DM8 O_3 are much greater than those of the corresponding annual mean DM8 O_3, indicating the impact of emission reductions in the region on reducing peak O_3 during regional pollution episodes. During the period 2000-2007 when solely VOC emissions reduced (-10%), no significant reduction in either annual maximum or average of DM8 O_3 occurred. Reductions in NO_x (-10%) with VOC (-5%) emissions in the subsequent 2007 to 2010 period lead to reductions in both maximum and average of DM8 O_3.

4.2 PM chemistry

The nonlinear response of NO_3^- concentration to SO_2, NO_x and NH_3 emissions are well documented (e.g., Mathur and Dennis, 2003; Tsimpidi et al., 2007; Makar et al., 2009). Fig. 11 attempts to summarize the changes in emissions and factors driving the NO_x-SO_x-NH_x system and its influence on changing inorganic particulate matter composition for the three regions. Contrasting trends in emissions over the past two decades in the three regions are apparent: while China and many growing regions of Asia have witnessed significant increases in emissions of NO_x, SO_2, and NH_3, significant reductions in emissions of all these species have occurred in Europe. In contrast in the eastern U.S., while combustion related emissions of NO_x and SO_2 have declined, growth in agricultural animal husbandry have resulted in significant increases in NH_3 emissions. To examine the impact of the varying emissions patterns on inorganic particulate matter formation and composition in these regions, we examined trends in two metrics relative to their 1990 values: (i) the degree of sulfate neutralization, an estimate of the neutralization of sulfate by ammonium (Pinder et al. (2008b); $DSN=([NH_4^+] - [NO_3^-]) / [SO_4^{2-}]$), and (ii) a new metric, the "nitration ratio (NR)" (i.e., NO_3^- concentration divided by NO_x emission) to represent

the relative amount of oxidized-N emissions that is eventually transformed to aerosol NO_3^-, changes in the ratio could thus be viewed as an indicator of the relative effectiveness of NO_x controls for given conditions. Fig. 11 presents the response of PM chemistry to the changes in emissions as indicated by the trends in these metric during the period 1990-2010.

In eastern China, simultaneous growth of NH_3 emission with SO_2/NO_x plays a very important role in the increases of SO_4^{2-} and NO_3^- concentrations (Wang et al., 2011b). During the period 1993-2002 the rate of increase in NH_3 emissions is greater than that of $NO_x+2\times SO_2$ emissions (representing the amount of NH_3 needed for complete neutralization) with a ratio of 1.1 (i.e., x% (NO_x+2SO_2) growth along with 1.1x% NH_3 growth on a basis of 1990 emission level). In these NH_3-rich conditions, both DSN and NR consequently exhibit an increasing trend, suggesting that sufficient NH_3 was available to neutralize the available and increasing aerosol SO_4^{2-} and also enable formation of particulate NO_3^-. The increasing trend in NR for this region also indicate that the simultaneous growth in emissions of both reduced and oxidized nitrogen results in greater fraction of NO_x being eventually transformed to particulate NO_3^-. After 2002, both DSN and NR decline when the growth of $NO_x+2\times SO_2$ emissions is faster than that of NH_3 (ratio of 0.9), resulting in the decline of the DSN and NR and eventually back to the 1990-levels.

In contrast, in the eastern US, both DSN and NR exhibit a steady-increase during the entire 21 year period, suggesting progressively NH_3-rich conditions stemming from both the increased NH_3 emissions as well as more free NH_3 being available due to reduced SO_4^{2-} levels associated with declining SO_2 emissions. Steadily increasing trends in NR values also suggest that increasing NH_3 levels offset the relative effectiveness of NO_x controls in reducing the relative fraction of aerosol NO_3^- formed from declining NO_x emissions.

Interestingly, in Europe simultaneous control of NH_3 along with NO_x and SO_2 emissions

yields an emission change ratio of 0.6 (i.e., x% (NO_x+2SO_2) reduction along with 0.6x% reduction of NH_3 on a basis of 1990 emission level). Though a slight increase of DSN is simulated during 1992-2003 resulting from faster growth of NO_x and SO_2 compared to NH_3, there is no discernable trend in the estimated NR suggesting comparatively greater control effectiveness in this region compared to the other two, due to the simultaneous control of NH_3 with combustion related emissions of NO_x and SO_2.

5. Conclusion

Trends in air quality across the northern hemisphere from 1990 to 2010 have been simulated by the WRF-CMAQ model driven with a representation of historical emission inventories derived from the EDGAR. Thorough comparison with several surface observation networks mostly in Europe and North America has been conducted. Significant contrasting changes in emissions have occurred across the northern hemisphere over the past two decades with reductions in North America and Western Europe resulting from control measures on combustion related sources and increases across large parts of Asia associated with economic and population growth. Model calculations show associated contrasting trends in air pollution across the northern hemisphere emphasizing the changing tropospheric composition of trace pollutants as well as the potentially changing background pollution levels in different regions resulting from changes in the amounts of long-range transported pollution. The model is generally able to capture the observed trends in air pollution and performance statistics are comparable with results from other studies in regions across the northern hemisphere. However, the model estimates still suffer from uncertainties in emissions (in regards to temporal variation and speciation), coarse spatial resolution, and subsequent impacts on representation of non-linear atmospheric chemistry. The lightening NO_x emissions used in this studies (Price et al, 1997) are

likely overestimated by 0.5 to 5 times compared to a more recent study (Schumann and Huntrieser et al., 2007) and may contribute to some extent to the overestimation of NO_x, O_3 and nitrate concentrations. The trend of biogenic emissions, which hasn't been considered in this study, might also impact the analysis. The lack of long-term observations in Asia, particularly over China and India, limits a robust model performance evaluation as well as O_3 and PM chemistry assessment in these polluted areas. To future explore the limitation of coarse spatial resolution, we are currently conducting a study with a finer-scale simulation over the CONUS domain for the same simulated period as from 1990 to 2010. A detailed description and comparison will be provided in a separate paper (Gan et al., in preparation).

Model simulated air quality trends over the past two decades largely agree with those derived from observations. Significant reduction in ambient levels of most pollutants is seen in the U.S. and Europe resulting from emission controls implemented during 1990-2010, while levels of all pollutants in China show pronounced increasing trends during the same period. Examining the simulated and observed historical trends in atmospheric chemistry can help guide development of future air pollution abatement strategies. Model calculations over the 1990-2010 period suggest that in the relative amounts of VOC and NO_x emission controls in different regions across the northern hemisphere (east U.S., Europe, and China), have led to significantly different trends in tropospheric O_3 in these regions. In particular, steady increase in NO_x and VOC emissions (with a ratio of 0.46 relative to 1990 emissions) in China have resulted in a near-linear increase in surface O_3 concentrations in the region, suggesting that possible control strategies that maintain this relative ratio could potentially be most effective in avoiding non-linear response resulting from VOC-limitation of alternate approaches. Differences in the historical changes in the relative amounts of NH_3, NO_x, and SO_2 emissions in these regions also

impact the trends in inorganic particulate matter amounts and composition in these regions. In particular, the amount of particulate nitrate formed per unit of NO_x emissions is influenced by changing NH_3 emissions and could be important in assessing the relative effectiveness of different control strategies. Simultaneous growth of NH_3 emission along with those of NO_x and SO_2 in China over the past 2 decades has resulted in the increasing particulate nitrate formation trends in the region. In contrast, in the eastern U.S. the relative fraction of NO_x converted to particulate nitrate exhibits a steady increase over the past two decades suggesting an offset in the relative effectiveness of control measures on particulate nitrate levels in the region. Simultaneous reductions in NH_3 emissions along with those of NO_x, and SO_2 in west Europe over the past two decades resulted in no significant trend in nitration ratio, suggesting effectiveness of the overall measures in terms of particulate nitrate levels in the region.

Acknowledgements

Although this work has been reviewed and approved for publication by the U.S. Environmental Protection Agency (EPA), it does not reflect the views and policies of the agency. This work was supported in part by an inter-agency agreement between the U.S. Department of Energy project (IA number is DE-SC000378) and the U.S. EPA (IA number is RW-89-9233260 1). This research was performed while Jia Xing held a National Research Council Research Associateship Award at US EPA. The authors gratefully acknowledge the free availability and use of datasets associated with the EDGAR, SMOKE, GEIA, CASTNET, IMPROVE, AQS, EMEP, AIRBASE, WDCGG and China API initiatives.

References

Akimoto, H., Ohara, T., Kurokawa, J. I., and Horii, N.: Verification of energy consumption in China during 1996–2003 by using satellite observational data. Atmospheric Environment, 40(40), 7663-7667. 2006.

Appel, K. W., Gilliland, A. B., Sarwar, G., and Gilliam, R. C.: Evaluation of the Community Multiscale Air Quality (CMAQ) model version 4.5: sensitivities impacting model performance: part I—ozone. Atmospheric Environment, 41(40), 9603-9615, 2007.

Appel, K. W., Bhave, P. V., Gilliland, A. B., Sarwar, G., and Roselle, S. J.: Evaluation of the community multiscale air quality (CMAQ) model version 4.5: sensitivities impacting model performance; Part II—Particulate matter. Atmospheric Environment, 42(24), 6057-6066, 2008.

Binkowski, F. S. and Roselle, S.J.: Community Multiscale Air Quality (CMAQ) model aerosol component, I: Model description, Journal of Geophysical Research, 108, 4183, doi:10.1029/2001JD001409, 2003.

Blanchard, C. L., Tanenbaum, S., Hidy, G. M.: Effects of Sulfur Dioxide and Oxides of Nitrogen Emission Reductions on Fine Particulate Matter Mass Concentrations: Regional Comparisons. J. Air Waste Manage. Assoc., 57, 1337–1350, 2007.

Butler, T. J., and Lakens, G. E.: The impact of changing regional emissions on precipitation chemistry in the eastern United States. Atmospheric Environment. Part A. General Topics, 25(2), 305-315, 1991

Byun, D. and Schere, K. L.: Review of the governing equations, computational algorithms, and other components of the Models-3 Community Multiscale Air Quality (CMAQ) modeling

system, Appl. Mech. Rev., 59, 51–77, 2006.

Chameides, W. L., Fehsenfeld, F., Rodgers, M. O., Cardelino, C., Martinez, J., Parrish, D., Lonneman, W., Lawson, D.R., Rasmussen, R.A., Zimmerman, P., Greenberg, J., Mlddleton, P. and Wang, T.: Ozone precursor relationships in the ambient atmosphere. Journal of Geophysical Research: Atmospheres (1984–2012), 97(D5), 6037-6055, 1992.

Civerolo, K., Hogrefe, C., Zalewsky, E., Hao, W., Sistla, G., Lynn, B., Rosenzweig, C., Kinney, P. L.: Evaluation of an 18-year CMAQ simulation: Seasonal variations and long-term temporal changes in sulfate and nitrate. Atmos. Environ., 44, 4745−3752, 2010.

Colette, A., Granier, C., Hodnebrog, Ø., Jakobs, H., Maurizi, A., Nyiri, A., Bessagnet, B., D'Angiola, A., D'Isidoro, M., Gauss, M., Meleux, F., Memmesheimer, M., Mieville, A., Rouïl, L., Russo, F., Solberg, S., Stordal, F., and Tampieri, F.: Air quality trends in Europe over the past decade: a first multi-model assessment, Atmos. Chem. Phys., 11, 11657-11678, doi:10.5194/acp-11-11657-2011, 2011.

Cong, Z., Kang, S., Gao, S., Zhang, Y., Li, Q., and Kawamura, K.: Historical trends of atmospheric black carbon on Tibetan Plateau as reconstructed from a 150-year lake sediment record. Environmental science & technology, 47(6), 2579-2586, 2013.

Ding, A. J., Wang, T., Thouret, V., Cammas, J.-P., and Nédélec, P.: Tropospheric ozone climatology over Beijing: analysis of aircraft data from the MOZAIC program, Atmos. Chem. Phys., 8, 1-13, doi:10.5194/acp-8-1-2008, 2008.

Eder, B. and Yu, S.: A performance evaluation of the 2004 release of Models-3 CMAQ, Atmospheric Environment, 40, 4811-4824, 2006.

EEA (European Environment Agency): European Union emission inventory report 1990–2010 under the UNECE Convention on Long-range Transboundary Air Pollution (LRTAP), EEA

Technical report, 30 Jul, Copenhagen, Denmark, doi:10.2800/5219, 2012.

European Commission: Joint Research Centre (JRC)/Netherlands Environmental Assessment Agency (PBL). Emission Database for Global Atmospheric Research (EDGAR), release version 4.2., available at: http://edgar.jrc.ec.europa.eu (last access: 25 September 2014), 2011.

Foley, K. M., Roselle, S. J., Appel, K. W., Bhave, P. V., Pleim, J. E., Otte, T. L., Mathur, R., Sarwar, G., Young, J. O., Gilliam, R. C., Nolte, C. G., Kelly, J. T., Gilliland, A. B., and Bash, J. O.: Incremental testing of the Community Multiscale Air Quality (CMAQ) modeling system version 4.7, Geosci. Model Dev., 3, 205–226, doi:10.5194/gmd-3-205-2010, 2010.

Gan, C.-M., Pleim, J., Mathur, R., Hogrefe, C., Long, C. N., Xing, J., Roselle, S., and Wei, C.: Assessment of the effect of air pollution controls on trends in shortwave radiation over the United States from 1995 through 2010 from multiple observation networks, Atmos. Chem. Phys., 14, 1701–1715, 2014.

Gan, C.-M., Pleim, J., Mathur, R., Hogrefe, C., Long, C.N., Xing, J., Wong, D., Gilliam, R., Roselle, S.J. and Wei, C.: Assessment of long-term simulations with various observations for better understanding of aerosol effects on radiation “brightening” in the United States, in preparation.

Guenther, A., Hewitt, C. N., Erickson, D., Fall, R., Geron, C., Graedel, T., Harley, P., Klinger, L., Lerdau, M., McKay, W. A., Pierce, T., Scholes, B., Steinbrecher, R., Tallamraju, R., Taylor, J., and Zimmerman, P.: A Global Model of Natural Volatile Organic Compound Emissions, J. Geophys. Res., 100, 8873–8892, 1995.

He, K. B.: Multi-resolution Emission Inventory for China (MEIC): model framework and 1990–2010 anthropogenic emissions, International Global Atmospheric Chemistry Conference,

17–21 September, Beijing, China, S1-I-2, 2012.

Heald, C. L., J. L. Collett Jr., Lee, T., Benedict, K. B., Schwandner, F. M., Li, Y., Clarisse, L., Hurtmans, D. R., Van Damme, M., Clerbaux, C., Coheur, P.-F., Philip, S., Martin, R. V., and Pye, H. O. T.: Atmospheric ammonia and particulate inorganic nitrogen over the United States, Atmos. Chem. Phys., 12, 10295-10312, doi:10.5194/acp-12-10295-2012, 2012.

Hogrefe, C., Lynn, B., Goldberg, R., Rosenzweig, C., Zalewsky, E., Hao, W., Doraiswamy, P., Civerolo, K., Ku, J.-Y., Sistla, G., and Kinney, P.L.: A combined model-observation approach to estimate historic gridded fields of $PM_{2.5}$ mass and species concentrations. Atmospheric Environment 43, 2561-2570, 2009.

Hogrefe, C., Hao, W., Zalewsky, E. E., Ku, J.-Y., Lynn, B., Rosenzweig, C., Schultz, M. G., Rast, S., Newchurch, M. J., Wang, L., Kinney, P. L., and Sistla, G.: An analysis of long-term regional-scale ozone simulations over the Northeastern United States: variability and trends, Atmos. Chem. Phys., 11, 567-582, doi:10.5194/acp-11-567-2011, 2011.

Iacono, M.J., Delamere, J.S., Mlawer, E.J., Shephard, M.W., Clough, S.A., and Collins, W.D.: Radiative forcing by long-lived greenhouse gases: Calculations with the AER radiative transfer models, J. Geophys. Res., 113, D13103, doi:10.1029/2008JD009944, 2008.

Irie, H., Sudo, K., Akimoto, H., Richter, A., Burrows, J.P., Wagner, T., Wenig, M., Beirle, S., Kondo, Y., Sinyakov, V.P. and Goutail, F.: Evaluation of long-term tropospheric NO2 data obtained by GOME over East Asia in 1996–2002. Geophysical Research Letter 32(11), L11810, doi: 10.1029/2005GL022770, 2005.

Jaffe, D., and Ray, J.: Increase in surface ozone at rural sites in the western US. Atmospheric Environment, 41(26), 5452-5463, 2007.

Janssens-Maenhout, G., Dentener, F., Van Aardenne, J., Monni, S., Pagliari, V., Orlandini, L., Klimont, Z., Kurokawa, J., Akimoto, H., Ohara, T.,Wankmueller, R., Battye, B., Grano, D., Zuber, A., and Keating, T.: EDGAR-HTAP: a Harmonized Gridded Air Pollution Emission Dataset Based on National Inventories, European Commission Publications Office, Ispra, Italy, EUR report No EUR 25229, 2012.

Järvi, L., Junninen, H., Karppinen, A., Hillamo, R., Virkkula, A., Mäkelä, T., Pakkanen, T., and Kulmala, M.: Temporal variations in black carbon concentrations with different time scales in Helsinki during 1996–2005, Atmos. Chem. Phys., 8, 1017-1027, doi:10.5194/acp-8-1017-2008, 2008.

Jiang, D.H., Zhang, Y., Hu, X., Zeng, Y., Tan, J.G., Shao, D.M.:Progress in developing an ANN model for air pollution index forecasting, Atmospheric Environment, 28, pp. 7055–7064, 2004.

Koumoutsaris, S. and Bey, I.: Can a global model reproduce observed trends in summertime surface ozone levels? Atmos. Chem. Phys., 12, 6983–6998, doi:10.5194/acp-12-6983-2012, 2012.

Kukkonen, J., Olsson, T., Schultz, D. M., Baklanov, A., Klein, T., Miranda, A. I., Monteiro, A., Hirtl, M., Tarvainen, V., Boy, M., Peuch, V.-H., Poupkou, A., Kioutsioukis, I., Finardi, S., Sofiev, M., Sokhi, R., Lehtinen, K. E. J., Karatzas, K., San José, R., Astitha, M., Kallos, G., Schaap, M., Reimer, E., Jakobs, H., and Eben, K.: A review of operational, regional-scale, chemical weather forecasting models in Europe, Atmos. Chem. Phys., 12, 1-87, doi:10.5194/acp-12-1-2012, 2012.

Logan, J. A., Staehelin, J., Megretskaia, I. A., Cammas, J.-P., Thouret, V., Claude, H., De Backer, H., Steinbacher, M., Scheel, H. E., St¨ubi, R., Fr¨ohlich, M., and Derwent, R.: Changes in

ozone over Europe: analysis of ozone measurements from sondes, regular aircraft (MOZAIC) and alpine surface sites, J. Geophys. Res., 117, D09301, doi:10.1029/2011JD016952, 2012.

Luo, C., Wang, Y.H., Mueller, S., and Knipping, E.: Diagnosis of an underestimation of summertime sulfate using the Community Multiscale Air Quality model. Atmos Environ, 45, 5119–30, 2011.

Makar, P. A., Moran, M. D., Zheng, Q., Cousineau, S., Sassi, M., Duhamel, A., Besner, M., Davignon, D., Crevier, L.-P., and Bouchet, V. S.: Modelling the impacts of ammonia emissions reductions on North American air quality, Atmos. Chem. Phys., 9, 7183-7212, doi:10.5194/acp-9-7183-2009, 2009.

Mathur, R., and Dennis, R. L.: Seasonal and annual modeling of reduced nitrogen compounds over the eastern United States: Emissions, ambient levels, and deposition amounts. Journal of Geophysical Research: Atmospheres (1984–2012), 108, 4481, doi:10.1029/2002JD002794, 2003.

Mathur, R., Yu, S., Kang, D., and Schere, K. L.: Assessment of the wintertime performance of developmental particulate matter forecasts with the Eta‐Community Multiscale Air Quality modeling system. Journal of Geophysical Research: Atmospheres (1984‐2012), 113, D02303, doi:10.1029/2007JD008580, 2008.

Mathur, R., Gilliam, R., Bullock, O.R., Roselle, S., Pleim, J., Wong, D., Binkowski, F., and Streets, D.: Extending the applicability of the community multiscale air quality model to hemispheric scales: motivation, challenges, and progress. In: Steyn DG, Trini S (eds) Air pollution modeling and its applications, XXI. Springer, Dordrecht, pp 175–179, 2012.

Mathur, R., Roselle, S., Young, J. and Kang, D.: Representing the Effects of Long-Range

Transport and Lateral Boundary Conditions in Regional Air Pollution Models, Air Pollution Modeling and its Application XXII NATO Science for Peace and Security Series C: Environmental Security, Springer, Heidelburg, Germany, Chapter 51, 303-308, 2014.

Matthias, V., Aulinger, A., Bieser, J., Cuesta, J., Geyer, B., Langmann, B., Serikov, I., Mattis, I., Minikin, A., Mona, L., Quante, M., Schumann, U., and Weinzierl, B.: The ash dispersion over Europe during the Eyjafjallajökull eruption—comparison of CMAQ simulations to remote sensing and air-borne in-situ observations. Atmos. Environ. 48, 184–194, 2012.

Ott, L. E., Pickering, K. E., Stenchikov, G. L., Allen, D. J., De-Caria, A. J., Ridley, B., Lin, R.-F., Lang, S., and Tao, W.-K.: Production of lightning NO(x) and its vertical distribution calculated from three-dimensional cloud-scale chemical transport model simulations, J. Geophys. Res.-Atmos., 115, D04301, doi:10.1029/2009jd011880, 2010.

Parrish, D. D., Millet, D. B., and Goldstein, A. H.: Increasing ozone in marine boundary layer inflow at the west coasts of North America and Europe, Atmos. Chem. Phys., 9, 1303-1323, doi:10.5194/acp-9-1303-2009, 2009.

Parrish, D. D., Law, K. S., Staehelin, J., Derwent, R., Cooper, O. R., Tanimoto, H., Volz-Thomas, A., Gilge, S., Scheel, H.-E., Steinbacher, M., and Chan, E.: Long-term changes in lower tropospheric baseline ozone concentrations at northern mid-latitudes, Atmos. Chem. Phys., 12, 11485-11504, doi:10.5194/acp-12-11485-2012, 2012.

Parrish, D. D., Lamarque, J. F., Naik, V., Horowitz, L., Shindell, D. T., Staehelin, J., Derwent, R., Cooper, O.R., Tanimoto, H., Volz-Thomas, A., Gilge, S., Scheel, H.-E., Steinbacher, M., and Fröhlich, M.: Long‐term changes in lower tropospheric baseline ozone concentrations: Comparing chemistry‐climate models and observations at northern midlatitudes. Journal of Geophysical Research: Atmospheres, 119(9), 5719-5736, 2014.

Price, C., Penner, J., and Prather, M.: NOx from lightning 1: Global distribution based on lightning physics, J. Geophys. Res., 102(D5), 5929–5941, 1997.

Pleim, J. E. and Xiu, A.: Development and testing of a surface flux and planetary boundary layer model for application in mesoscale models. J. Appl. Meteor., 34, 16–32, 1995.

Pleim, J. E. and Xiu, A.: Development of a land surface model. Part II: Data Assimilation. J. Appl. Meteor., 42, 1811–1822, 2003.

Pleim, J. E.: A Combined Local and Nonlocal Closure Model for the Atmospheric Boundary Layer. Part I: Model Description and Testing, J. Appl. Meteorol. Climatol., 46, 1383–1395, doi:10.1175/JAM2539.1, 2007a.

Pleim, J. E.: A Combined Local and Nonlocal Closure Model for the Atmospheric Boundary Layer. Part II: Application and Evaluation in a Mesoscale Meteorological Model, J. Appl. Meteorol. Climatol., 46, 1396–1409, doi:10.1175/JAM2534.1, 2007b.

Pleim J. E. and R. Gilliam: An indirect data assimilation scheme for deep soil temperature in the Pleim-Xiu land surface model. J. Appl. Meteor. Clim., 48, 1362-1376, 2009.

Richter, A., Burrows, J. P., Nues, H., Granier, C., and Niemeier, U.: Increase in tropospheric nitrogen dioxide over China observed from space, Nature, 437, 129–132, 2005.

Pandis, S. N. and Seinfeld, J. H.: Sensitivity analysis of a chemical mechanism for aqueous‐phase atmospheric chemistry. Journal of Geophysical Research: Atmospheres (1984‐2012), 94(D1), 1105-1126, 1989.

Pinder, R. W., Gilliland, A. B. and Dennis, R. L.: Environmental impact of atmospheric NH3 emissions under present and future conditions in the eastern United States, Geophys. Res. Lett., 35, L12808, doi:10.1029/2008GL033732, 2008a.

Pinder, R. W., Dennis, R. L., and Bhave, P. V.: Observable indicators of the sensitivity of PM<

sub> 2.5</sub> nitrate to emission reductions—Part I: Derivation of the adjusted gas ratio and applicability at regulatory-relevant time scales. Atmospheric Environment, 42(6), 1275-1286, 2008b.

Schumann, U. and Huntrieser, H.: The global lightning-induced nitrogen oxides source, Atmos. Chem. Phys., 7, 3823-3907, doi:10.5194/acp-7-3823-2007, 2007.

Sharma, S., Lavoué, D., Cachier, H., Barrie, L. A., and Gong, S. L.: Long - term trends of the black carbon concentrations in the Canadian Arctic. Journal of Geophysical Research: Atmospheres (1984 – 2012), 109, D15203, doi:10.1029/2003JD004331, 2004.

Sickles, J.E., II, and Shadwick, D.S.: Changes in air quality and atmospheric deposition in the eastern United States: 1990-2004. J.Geophys. Res., 112, D17302, doi: 10.1029/2006JD007843, 2007.

Sillman, S.: The relation between ozone, NOx and hydrocarbons in urban and polluted rural environments, Atmos. Environ., 33, 1821–1845, 1999.

Simpson D., Fagerli, H., Jonson, J.E., Tsyro, S., Wind, P., and Tuovinen, J.: "Transboundary Acidification, Eutrophication, and Ground Level Ozone in Europe – Part I: Unified EMEP Model Description." EMEP Status Report 2003, The Norwegian Meteorological Institute, Oslo, 25 Norway, 2003.

Tesche, T.W., Morris, R., Tonnesen, G., McNally, D., Boylan, J., Brewer, P.: CMAQ/CAMx annual 2002 performance evaluation over the eastern United States. Atmospheric Environment 40, 4906–4919, 2006.

Trainer, M., Parrish, D. D., Buhr, M. P., Norton, R. B., Fehsenfeld, F. C., Anlauf, K. G., Bottenheim, J.W., Tang, Y.Z., Wiebe, H.A., Roberts, J.M., Tanner, R.L., Newman, L., Bowersox, V.C., Meagher, J.F., Olszyna, K.J., Rodgers, M.O., Wang, T., Berresheim, H.,

Demerjian, K.L. and Roychowdhury, U. K.: Correlation of ozone with NOy in photochemically aged air. Journal of Geophysical Research: Atmospheres (1984–2012), 98(D2), 2917-2925, 1993

Tsimpidi, A.P., Karydis, V.A., and Pandis, S.N.: Response of Inorganic Fine Particulate Matter to Emission Changes of Sulfur Dioxide and Ammonia: The Eastern United States as a Case Study, J. Air & Waste Manage. Assoc. 57:1489–1498, DOI:10.3155/1047-3289.57.12.1489, 2007.

Wakamatsu, S., Morikawa, T. and Ito, A.: Air Pollution Trends in Japan between 1970 and 2012 and Impact of Urban Air Pollution Countermeasures, Asian Journal of Atmospheric Environment, Vol. 7-4, pp.177-190, December, 2013

Wang, K., Zhang, Y., Jang, C., Phillips, S., and Wang, B.: Modeling intercontinental air pollution transport over the trans‐Pacific region in 2001 using the Community Multiscale Air Quality modeling system. Journal of Geophysical Research: Atmospheres (1984‐2012), 114, D04307, doi:10.1029/2008JD010807, 2009

Wang, S., Xing, J., Chatani, S., Hao, J., Klimont, Z., Cofala, J., and Amann, M.: Verification of anthropogenic emissions of China by satellite and ground observations. Atmospheric Environment, 45(35), 6347-6358, 2011a.

Wang S., Xing J, Jang C, Zhu Y, Fu J, and Hao J.: Impact assessment of ammonia emissions on inorganic aerosols in east China using response surface modeling technique. Environmental Science and Technology, 45, 9293–9300, DOI: 10.1021/es2022347, 2011b.

Wang, S., Xing, J., Zhao, B., Jang, C., and Hao, J.: Effectiveness of national air pollution control policies on the air quality in metropolitan areas of China. Journal of Environmental Sciences, 26(1), 13-22, 2014.

Wang, Y., Konopka, P., Liu, Y., Chen, H., Müller, R., Plöger, F., Riese, M., Cai, Z., and Lü, D.: Tropospheric ozone trend over Beijing from 2002–2010: ozonesonde measurements and modeling analysis, Atmos. Chem. Phys., 12, 8389-8399, doi:10.5194/acp-12-8389-2012, 2012.

Wild, M.: Global dimming and brightening: A review, Journal of Geophysical Research, 114, D00D16, doi: 10.1029/2008JD011470, 2009.

Xing, J., Zhang, Y., Wang, S., Liu, X., Cheng, S., Zhang, Q., Chen, Y., Hao, J. and Wang, W.: Modeling study on the air quality impacts from emission reductions and atypical meteorological conditions during the 2008 Beijing Olympics. Atmospheric Environment, 45(10), 1786-1798, 2011a.

Xing, J., Wang, S. X., Jang, C., Zhu, Y., and Hao, J. M.: Nonlinear response of ozone to precursor emission changes in China: a modeling study using response surface methodology, Atmos. Chem. Phys., 11, 5027-5044, doi:10.5194/acp-11-5027-2011, 2011b.

Xing, J., Pleim, J., Mathur, R., Pouliot, G., Hogrefe, C., Gan, C.-M., and Wei, C.: Historical gaseous and primary aerosol emissions in the United States from 1990 to 2010, Atmos. Chem. Phys., 13, 7531-7549, doi:10.5194/acp-13-7531-2013, 2013.

Xiu, A. and J.E. Pleim: Development of a Land Surface Model. Part I: Application in a Mesoscale Meteorological Model. J. Appl. Meteor. 40:192-209, 2001.

Xu, X., and Lin, W.: Trends of Tropospheric Ozone over China Based on Satellite Data (1979—2005), Advances in Climate Change Research, 2, 43-48, 2011.

Yamaji, K., Ohara, T., Uno, I., Tanimoto, H., Kurokawa, J. I., and Akimoto, H.: Analysis of the seasonal variation of ozone in the boundary layer in East Asia using the Community Multi-scale Air Quality model: What controls surface ozone levels over Japan?. Atmospheric

Environment, 40(10), 1856-1868, 2006.

Zhang, H., Chen, G., Hu, J., Chen, S.-H., Wiedinmyer, C., Kleeman, M., and Ying, Q.: Evaluation of a seven-year air quality simulation using the Weather Research and Forecasting (WRF)/Community Multiscale Air Quality (CMAQ) models in the eastern United States, Science of The Total Environment, Volumes 473–474, 1 March, Pages 275–285, 2014.

Zhang, X., Zhang, P., Zhang, Y., Li, X., and Qiu, H.: The trend, seasonal cycle, and sources of tropospheric NO2 over China during 1997–2006 based on satellite measurement. Science in China Series D: Earth Sciences, 50(12), 1877-1884, 2007.

Zhang, X., van Geffen, J., Liao, H., Zhang, P., and Lou, S. J.: Spatiotemporal variations of tropospheric SO2 over China by SCIAMACHY observations during 2004−2009. Atmos. Environ., 60, 238−246, 2012.

Zhang, Y., Vijayaraghavan, K., Wen, X.-Y., Snell, H. E., and Jacobson, M. Z.: Probing into regional ozone and particulate matter pollution in the United States: 1. A 1 year CMAQ simulation and evaluation using surface and satellite data, J. Geophys. Res., 114, D22304, doi:10.1029/2009JD011898, 2009.

Zhao B, Wang S X, Dong X Y, Wang J D, Duan L, Fu X, Hao, J., and Fu, J.: Environmental effects of the recent emission changes in China: Implications for particulate matter pollution and soil acidification. Environmental Research Letters, 8, 24031, doi:10.1088/1748-9326/8/2/024031, 2013.

Table 1 Summary of long-term observations used for trends analysis in this study

Species	Network	Region	Number of sites (at least 18-year available with >75% annual coverage)	Time period	record frequency
Gaseous species					
SO_2	CASTNET	United States	38 selected from 133	1990-2010	Weekly
	AQS	United States	280 selected from 1177	1990-2010	Annual
	AIRBASE	Europe	126 selected from 510	1990-2010	Annual
	EMEP	Europe	44 selected from 237	1990-2010	Monthly
	API	China	7	2005-2010	Annual
NO_2	AQS	United States	181 selected from 714	1990-2010	Annual
	AIRBASE	Europe	160 selected from 440	1990-2010	Annual
	EMEP	Europe	39 selected from 237	1990-2010	Monthly
	API	China	7	2005-2010	Annual
O_3	CASTNET*	United States	25 selected from 133	1990-2010	Daily
	AIRBASE	Europe	147 selected from 315	1990-2010	Annual
	EMEP	Europe	69 selected from 190	1990-2010	Daily
	WDCGG	Global(Japan used only)	3 selected from 102	1990-2010	Hourly
Particles					
SO_4^{2-}	CASTNET	United States	38 selected from 133	1990-2010	Weekly
	IMPROVE	United States	27 selected from 197	1990-2010	Semi-weekly
	EMEP	Europe	39 selected from 237	1990-2010	Monthly
NO_3^-	CASTNET	United States	38 selected from 133	1990-2010	Weekly
	IMPROVE	United States	27 selected from 197	1990-2010	Semi-weekly
	EMEP	Europe	12 selected from 237	1990-2010	Monthly
NH_4^+	CASTNET	United States	38 selected from 133	1990-2010	Weekly
	EMEP	Europe	6 selected from 237	1990-2010	Monthly
EC	IMPROVE	United States	26 selected from 197	1990-2010	Semi-weekly

* There're few O_3 records from CASTNET in winter, thus criteria is set as at least 15 available years with >75% coverage from March to November for each year

Table 2 Model performance

(a) Gaseous species

Species	Network		Obs ($\mu g\ m^{-3}$)	R	MB ($\mu g\ m^{-3}$)	NMB (%)	RMSE ($\mu g\ m^{-3}$)	NME (%)	N pairs
SO_2	US-CASTNET	Spring	5.0	0.73	-1.1	-21.8	3.2	72.4	2316
		Summer	3.3	0.74	0.2	5.3	2.4	93.4	2352
		Fall	4.5	0.78	1.6	36.0	3.8	118.0	2348
		Winter	8.1	0.67	-2.7	-33.4	6.0	81.7	2317
		Annual	5.2	0.67	-0.5	-9.4	4.1	91.5	9333
	US-AQS	Annual	12.2	0.2	-4.6	-37.5	10.6	135.3	2628
	EU- AIRBASE	Annual	8.7	0.3	-1.5	-17.7	9.6	98.8	580
	EU-EMEP	Spring	2.4	0.43	2.0	82.2	5.0	239.8	2399
		Summer	1.6	0.44	2.4	150.1	4.7	325.0	2355
		Fall	2.2	0.48	2.2	102.7	4.9	324.1	2344
		Winter	3.8	0.50	0.1	3.6	5.2	177.6	2363
		Annual	2.5	0.43	1.7	67.0	5.0	266.3	9461
	CN-API	Annual	50.8	0.33	-18.4	-36.3	28.4	42.2	42
NO_2	US-AQS	Annual	29.0	0.2	-13.9	-47.9	22.6	63.4	1616
	EU- AIRBASE	Annual	32.0	0.4	-17.1	-53.5	22.5	55.9	747
	EU-EMEP	Spring	6.5	0.65	-0.1	-1.6	5.6	79.5	2049
		Summer	5.0	0.56	-0.7	-14.1	4.7	73.8	2066
		Fall	7.1	0.67	1.0	14.4	7.0	84.1	2084
		Winter	9.7	0.68	1.3	13.9	7.9	91.6	2068
		Annual	7.1	0.68	0.4	5.6	6.4	82.3	8267
	CN-API	Annual	46.6	0.08	-31.5	-67.5	36.1	66.2	42
O_3^*	US-CASTNET	Spring	168.1	0.52	-22.8	-13.6	29.7	16.1	1269
		Summer	176.8	0.59	-14.3	-8.1	30.5	14.5	1512
		Fall	155.3	0.60	-3.9	-2.5	23.5	12.4	1071
		Winter	112.5	0.51	-3.6	-3.2	10.1	7.6	217
	EU-AIRBASE	Annual	169.4	0.40	14.4	8.5	38.9	17.4	2776
	EU-EMEP	Spring	140.9	0.56	-2.1	-1.5	22.7	14.2	4145
		Summer	152.3	0.60	6.5	4.3	30.5	18.4	4161
		Fall	108.5	0.66	18.4	16.9	25.4	25.9	4151
		Winter	92.5	0.29	3.1	3.4	16.1	16.6	4111
	WDCGG-JP	Spring	165.4	0.68	-8.9	-5.4	26.1	14.4	175
		Summer	157.3	0.83	10.8	6.9	34.0	21.4	172
		Fall	128.5	0.62	17.4	13.5	31.4	21.9	173
		Winter	109.2	0.49	3.2	2.9	15.1	12.6	172

* Comparison of O_3 concentration is computed on the basis of annual or seasonal maximum of DM8 (daily 8-hour maxima) value, except that for AIRBASE which is computed on the basis of annual maxima of DM1 (daily 1-hour maxima)

(b) Fine particles

Species	Network		Obs ($\mu g\ m^{-3}$)	R	MB ($\mu g\ m^{-3}$)	NMB (%)	RMSE ($\mu g\ m^{-3}$)	NME (%)	N pairs
SO_4^{2-}	US-CASTNET	Spring	3.1	0.87	-0.2	-7.5	0.8	29.2	2316
		Summer	5.3	0.86	-2.4	-45.2	3.1	44.7	2352
		Fall	3.7	0.86	-1.0	-26.5	1.8	34.3	2348
		Winter	2.3	0.63	-0.8	-35.6	1.2	53.1	2316
		Annual	3.6	0.81	-1.1	-30.8	1.9	40.3	9332
	US- IMPROVE	Spring	1.4	0.89	0.3	22.5	0.7	70.3	1602
		Summer	2.2	0.90	-0.6	-28.9	1.8	37.8	1596
		Fall	1.3	0.90	0.2	15.7	0.7	68.4	1605
		Winter	0.9	0.76	0.1	16.3	0.6	106.7	1605
		Annual	1.4	0.85	0.0	0.7	1.1	70.8	6408
	EU- EMEP	Spring	2.6	0.68	0.3	12.5	1.4	52.3	2099
		Summer	2.4	0.68	0.1	3.7	1.3	41.4	2071
		Fall	2.2	0.64	0.0	1.9	1.4	55.9	2042
		Winter	2.4	0.53	-0.7	-28.6	1.9	58.3	2058
		Annual	2.4	0.61	-0.1	-2.4	1.5	51.9	8270
NO_3^-	US-CASTNET	Spring	1.1	0.69	1.0	92.9	2.1	195.5	2316
		Summer	0.4	0.31	-0.2	-48.2	0.4	76.1	2352
		Fall	0.7	0.68	0.1	13.8	0.7	99.3	2348
		Winter	1.6	0.71	1.2	75.2	1.9	262.0	2316
		Annual	0.9	0.72	0.5	56.4	1.5	157.7	9332
	US- IMPROVE	Spring	0.4	0.72	0.4	106.9	1.0	164.8	1602
		Summer	0.2	0.10	-0.1	-40.5	0.2	93.0	1596
		Fall	0.3	0.66	0.0	11.4	0.4	125.7	1604
		Winter	0.5	0.66	0.5	94.8	1.1	226.9	1605
		Annual	0.3	0.66	0.2	59.1	0.8	152.7	6407
	EU- EMEP	Spring	3.0	0.75	0.3	10.8	2.0	75.2	679
		Summer	1.8	0.74	-1.2	-67.0	1.5	74.7	656
		Fall	2.3	0.72	-0.4	-15.0	1.5	64.4	659
		Winter	2.6	0.64	0.6	23.1	2.1	91.2	671
		Annual	2.4	0.70	-0.2	-6.3	1.8	76.4	2665
NH_4^+	US-CASTNET	Spring	1.2	0.68	0.3	22.6	0.8	52.0	2316
		Summer	1.6	0.77	-0.8	-53.7	1.1	50.5	2352
		Fall	1.2	0.72	-0.3	-21.4	0.6	31.7	2348
		Winter	1.1	0.76	0.2	19.0	0.6	54.1	2316
		Annual	1.3	0.52	-0.2	-12.9	0.8	47.0	9332
	EU- EMEP	Spring	1.4	0.69	0.7	51.3	1.4	101.4	335
		Summer	1.2	0.64	-0.2	-15.2	0.9	43.9	330
		Fall	1.2	0.67	0.3	28.2	1.0	73.7	332
		Winter	1.1	0.62	0.8	68.4	1.4	110.4	328
		Annual	1.2	0.62	0.4	33.7	1.2	82.4	1325
EC	US- IMPROVE	Spring	0.2	0.79	-0.1	-62.5	0.2	62.7	1536
		Summer	0.3	0.54	-0.2	-73.5	0.3	92.7	1532
		Fall	0.3	0.81	-0.2	-64.4	0.3	65.9	1548
		Winter	0.2	0.85	-0.1	-59.4	0.2	55.7	1542
		Annual	0.2	0.74	-0.2	-65.1	0.3	69.2	6158

Table 3 Simulated trends in three regions (grid-averaged)

	Eastern China		Eastern US		Europe	
Emission	kg km^{-2} yr^{-1}	% yr^{-1}	kg km^{-2} yr^{-1}	% yr^{-1}	kg km^{-2} yr^{-1}	% yr^{-1}
SO_2	20.2	3.2	-16.1	-5.4	-20.4	-5.4
NO_x	8.5	4.3	-3.7	-1.8	-3.0	-1.5
VOC	18.6	2.3	-22.5	-3.3	-26.7	-3.3
NH_3	6.5	2.6	1.7	1.6	-2.6	-1.0
PM_{10}	2.1	0.3	-4.5	-4.6	-10.0	-4.8
Concentration	µg m^{-3} yr^{-1}	% yr^{-1}	µg m^{-3} yr^{-1}	% yr^{-1}	µg m^{-3} yr^{-1}	% yr^{-1}
SO_2	0.265	2.70	-0.175	-5.71	-0.178	-5.06
NO_2	0.119	4.14	-0.048	-1.38	-0.040	-1.16
*O_3	2.566	1.49	-1.028	-0.66	-0.875	-0.54
$PM_{2.5}$	0.481	2.21	-0.097	-1.21	-0.253	-2.62
SO_4^{2-}	0.185	2.82	-0.072	-3.17	-0.109	-3.73
NO_3^-	0.097	5.40	0.014	1.61	-0.030	-1.84
NH_4^+	0.081	3.44	-0.006	-0.72	-0.041	-2.91
EC	0.005	0.99	-0.004	-3.39	-0.005	-2.46

Colored entries are significant at p=0.05 level: green=significant decrease; orange=significant increase.

* Trend in O_3 is computed on the basis of annual or seasonal maximum of DM8 (daily 8-hour maxima) value

Table 4 Comparison of observed and simulated trend (unit: μg m^{-3} yr^{-1}, computed on the basis of annual and seasonal means over the 1990-2010 period with a linear least square fit method) and the annual change rate (x%, i.e., concentration in the year Y (C_Y) will be fit as $C_Y=C_{1990}\times(1+x)^{Y-1990}$)

Species	Network		Spring		Summer		Fall		Winter		Annual	
			obs	sim	obs	sim	obs	sim	obs	sim	obs	sim
SO_2	US-CASTNET	μg m^{-3}	-0.228	-0.238	-0.152	-0.204	-0.234	-0.385	-0.368	-0.366	-0.245	-0.298
		%	-4.74	-6.26	-4.91	-6.13	-5.61	-6.63	-4.79	-7.01	-4.98	-6.57
	US-AQS	μg m^{-3}									-0.626	-0.467
		%									-5.31	-6.45
	EU-AIRBASE	μg m^{-3}									-0.873	-0.441
		%									-8.86	-5.86
	EU-EMEP	μg m^{-3}	-0.187	-0.282	-0.108	-0.225	-0.180	-0.279	-0.339	-0.264	-0.204	-0.262
		%	-7.03	-6.16	-5.95	-5.53	-7.28	-6.23	-8.04	-6.28	-7.26	-6.05
	CN-API	μg m^{-3}									0.376	1.230
		%									0.66	4.02
NO_2	US-AQS	μg m^{-3}									-0.629	-0.311
		%									-2.3	-2.2
	EU-AIRBASE	μg m^{-3}									-0.640	-0.136
		%									-1.88	-0.86
	EU-EMEP	μg m^{-3}	-0.087	-0.113	-0.115	-0.137	-0.150	-0.194	-0.150	-0.195	-0.126	-0.160
		%	-1.29	-1.64	-2.26	-3.03	-2.00	-2.30	-1.46	-1.70	-1.69	-2.04
	CN-API	μg m^{-3}									-0.454	0.868
		%									-0.97	5.94
O_3*	US-CASTNET	μg m^{-3}	-1.187	-0.903	-1.860	-1.010	-1.220	-0.527	-0.029	-0.134	-1.859	-0.952
		%	-0.73	-0.65	-1.14	-0.68	-0.83	-0.36	-0.02	-0.13	-1.10	-0.64
	EU-AIRBASE	μg m^{-3}									-1.348	-2.129
		%									-0.79	-1.13
	EU-EMEP	μg m^{-3}	-0.651	-1.281	-1.207	-1.365	-0.157	-0.184	0.124	-0.048	-1.067	-1.313
		%	-0.46	-0.92	-0.85	-0.91	-0.13	-0.15	0.14	-0.05	-0.74	-0.87
	WDCGG-Minamitorishima	μg m^{-3}	0.485	-0.029	-1.131	-0.083	-0.688	0.090	-0.416	0.413	0.232	-0.126
		%	0.35	-0.02	-1.19	0.01	-0.70	0.09	-0.31	0.38	0.18	-0.11
	WDCGG- Ryori	μg m^{-3}	1.305	0.372	0.549	0.259	-0.638	0.308	0.166	0.217	0.702	0.440
		%	0.79	0.24	0.44	0.18	-0.47	0.25	0.24	0.23	0.41	0.29
	WDCGG-Tsukuba	μg m^{-3}	-1.073	-0.019	-4.015	-0.375	0.581	-1.017	-0.368	0.861	-3.299	-0.022
		%	-0.60	-0.02	-1.78	-0.18	0.52	-0.56	-0.31	0.74	-1.40	-0.01
SO_4^{2-}	US-CASTNET	μg m^{-3}	-0.070	-0.073	-0.161	-0.125	-0.112	-0.098	-0.054	-0.046	-0.099	-0.086
		%	-2.30	-2.49	-3.25	-4.45	-3.31	-3.75	-2.25	-3.01	-2.87	-3.46
	US-IMPROVE	μg m^{-3}	-0.023	-0.021	-0.049	-0.043	-0.036	-0.041	-0.024	-0.016	-0.033	-0.030
		%	-1.76	-1.24	-2.45	-2.86	-2.87	-2.69	-2.76	-1.59	-2.43	-2.11
	EU-EMEP	μg m^{-3}	-0.119	-0.086	-0.111	-0.112	-0.097	-0.085	-0.090	-0.060	-0.104	-0.086
		%	-4.28	-2.84	-4.35	-4.49	-4.27	-3.93	-3.39	-3.29	-4.06	-3.62
NO_3^-	US-CASTNET	μg m^{-3}	-0.009	0.023	-0.011	0.005	-0.015	0.023	0.009	0.057	-0.006	0.027
		%	-0.94	1.19	-3.17	3.38	-2.27	3.33	0.61	2.35	-0.73	2.10
	US-IMPROVE	μg m^{-3}	-0.002	0.012	-0.004	0.000	-0.005	0.010	-0.002	0.024	-0.003	0.012
		%	-0.70	1.93	-2.13	0.14	-1.97	3.73	-0.28	2.99	-1.04	2.53
	EU-EMEP	μg m^{-3}	-0.015	-0.086	-0.019	-0.032	-0.009	-0.043	0.013	-0.002	-0.008	-0.041
		%	-0.47	-2.49	-1.06	-5.38	-0.51	-2.19	0.50	-0.13	-0.33	-1.74
NH_4^+	US-CASTNET	μg m^{-3}	-0.023	-0.002	-0.038	-0.010	-0.032	-0.006	-0.013	0.012	-0.026	-0.002
		%	-2.04	-0.19	-2.60	-1.54	-2.86	-0.68	-1.24	0.97	-2.19	-0.18
	EU-EMEP	μg m^{-3}	0.003	-0.055	0.000	-0.049	0.020	-0.035	-0.002	-0.018	0.005	-0.039
		%	0.80	-2.22	0.30	-4.52	1.75	-2.21	0.16	-0.87	0.70	-2.19
EC	US-IMPROVE	μg m^{-3}	-0.005	-0.002	-0.003	-0.002	-0.009	-0.004	-0.008	-0.003	-0.006	-0.003
		%	-2.46	-2.77	-1.34	-3.42	-3.30	-3.67	-3.41	-3.32	-2.64	-3.32

Colored entries are significant at p=0.05 level: green=significant decrease; orange=significant increase.

* Trend in O_3 is computed on the basis of annual or seasonal maximum of DM8 (daily 8-hour maxima) value, except that for AIRBASE which is computed on the basis of annual maximum of DM1 (daily 1-hour maxima)

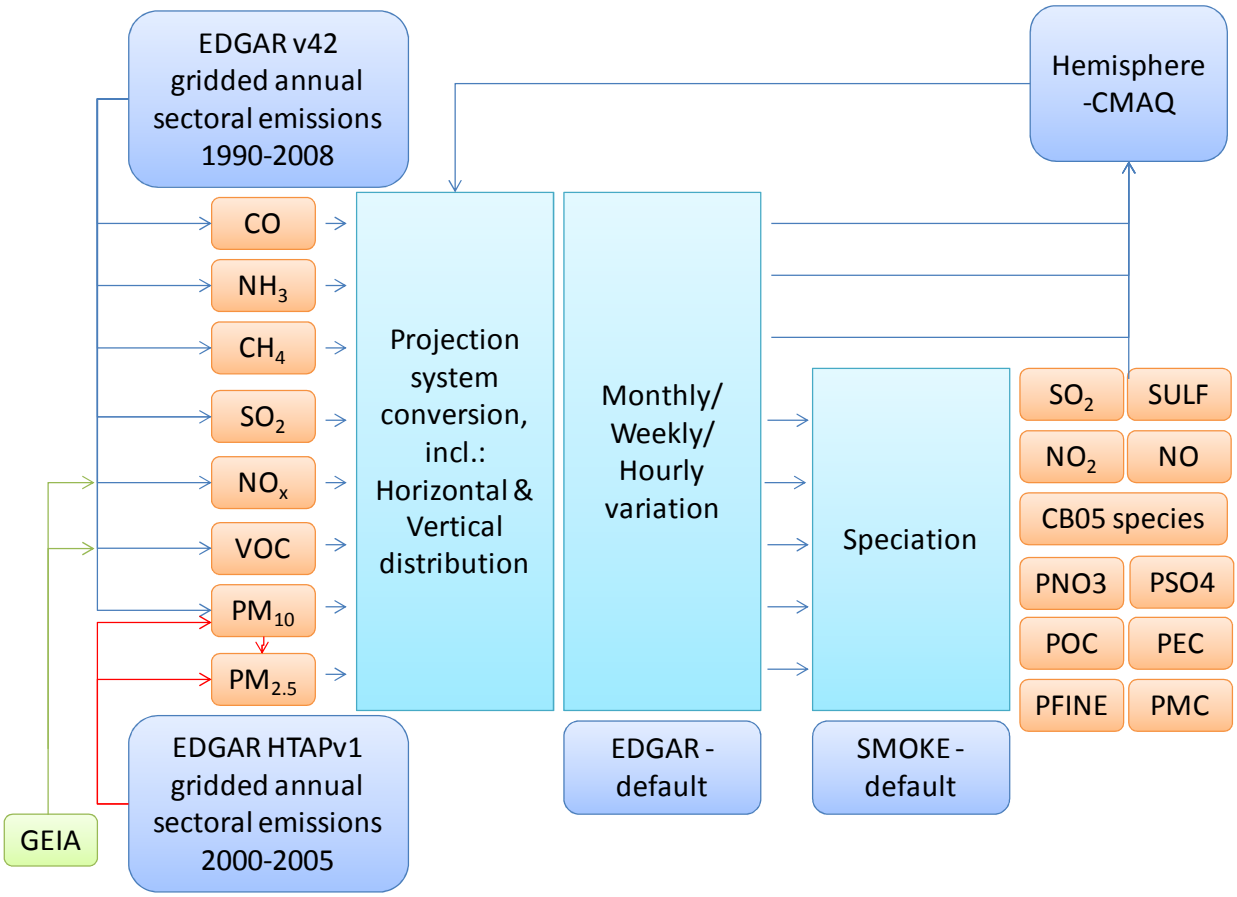

Fig. 1 Processes of gridded emissions for northern hemispheric WRF-CMAQ simulation

1

(a) SO_2 (b) NO_x

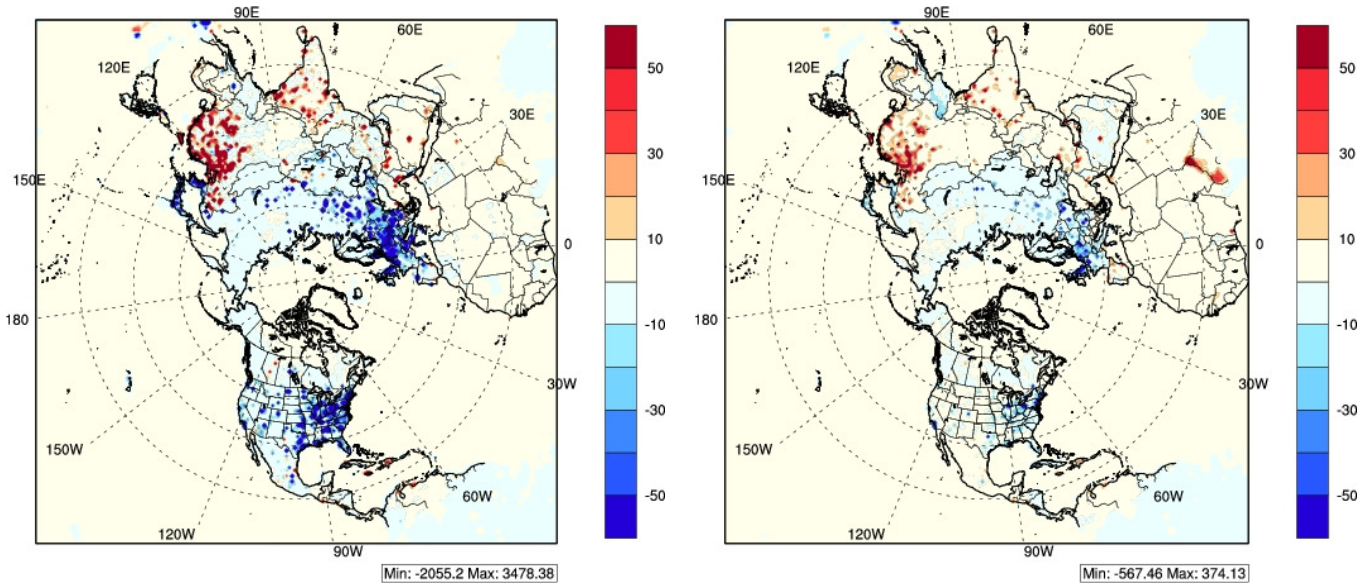

(c) NMVOC (d) NH_3

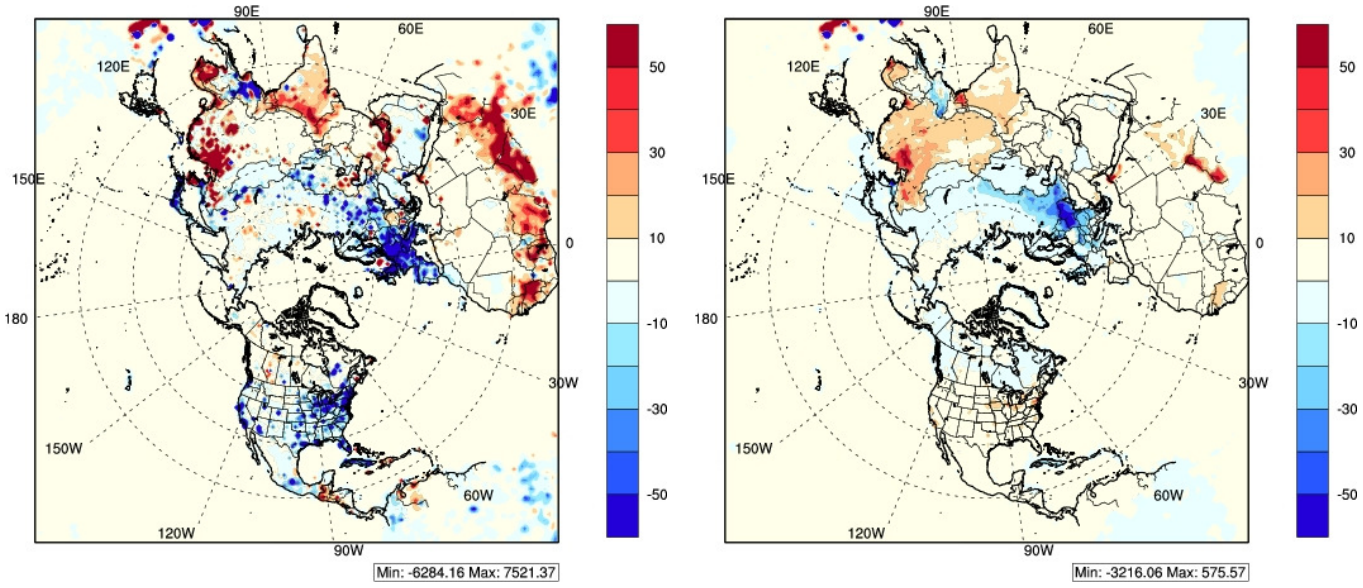

2

3 Fig. 2 EDGAR emission trend over 1990 to 2010 for SO_2, NO_x, NMVOC and NH_3

4 (unit: kg km^{-2} yr^{-1}, computed on the basis of annual means over the 1990-2010 period with a
5 linear least square fit method)

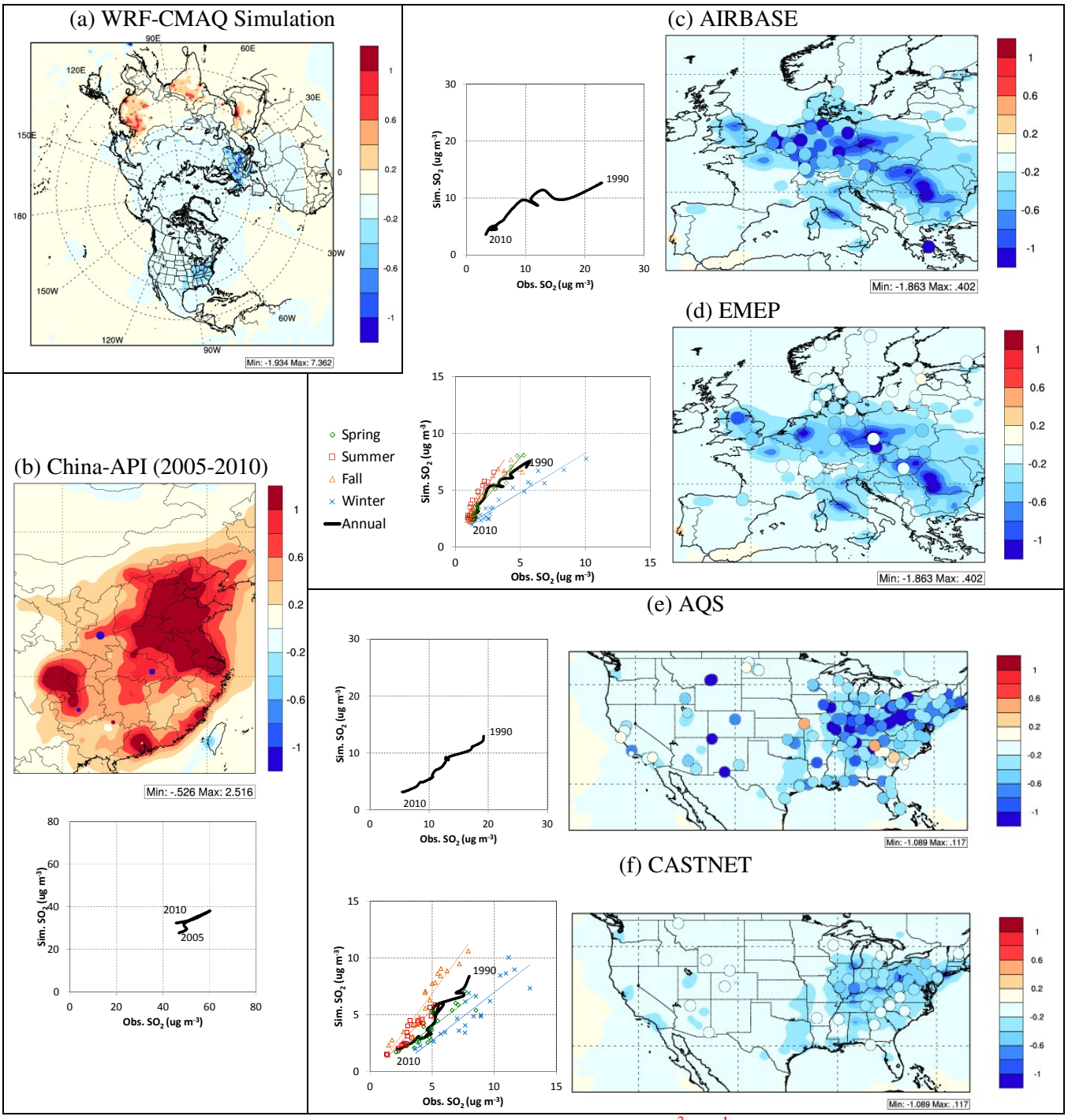

Fig. 3 (a) simulated SO_2 trend from WRF-CMAQ (unit: $\mu g m^{-3} yr^{-1}$); (b) upper-color map: simulated SO_2 trend in East China overlaid with observed SO_2 trend from China-API, dot represents each observation site, computed on the basis of annual means over the 2005–2010 period with a linear least square fit method, dot size is determined by the significance of trend, i.e., larger symbols denote more significant trends at 0.05 level (unit: $\mu g\ m^{-3}\ yr^{-1}$); lower-scatter plot: observed and simulated SO_2 concentration, network-mean for each year corresponding grid

cells from model simulation are selected for comparison (unit: μg m^{-3}); (c) same as (b) for Europe – AIRBASE; (d) same as (b) for Europe – EMEP; (e) same as (b) for the U.S. – AQS; (f) same as (b) for the U.S. – CASTNET

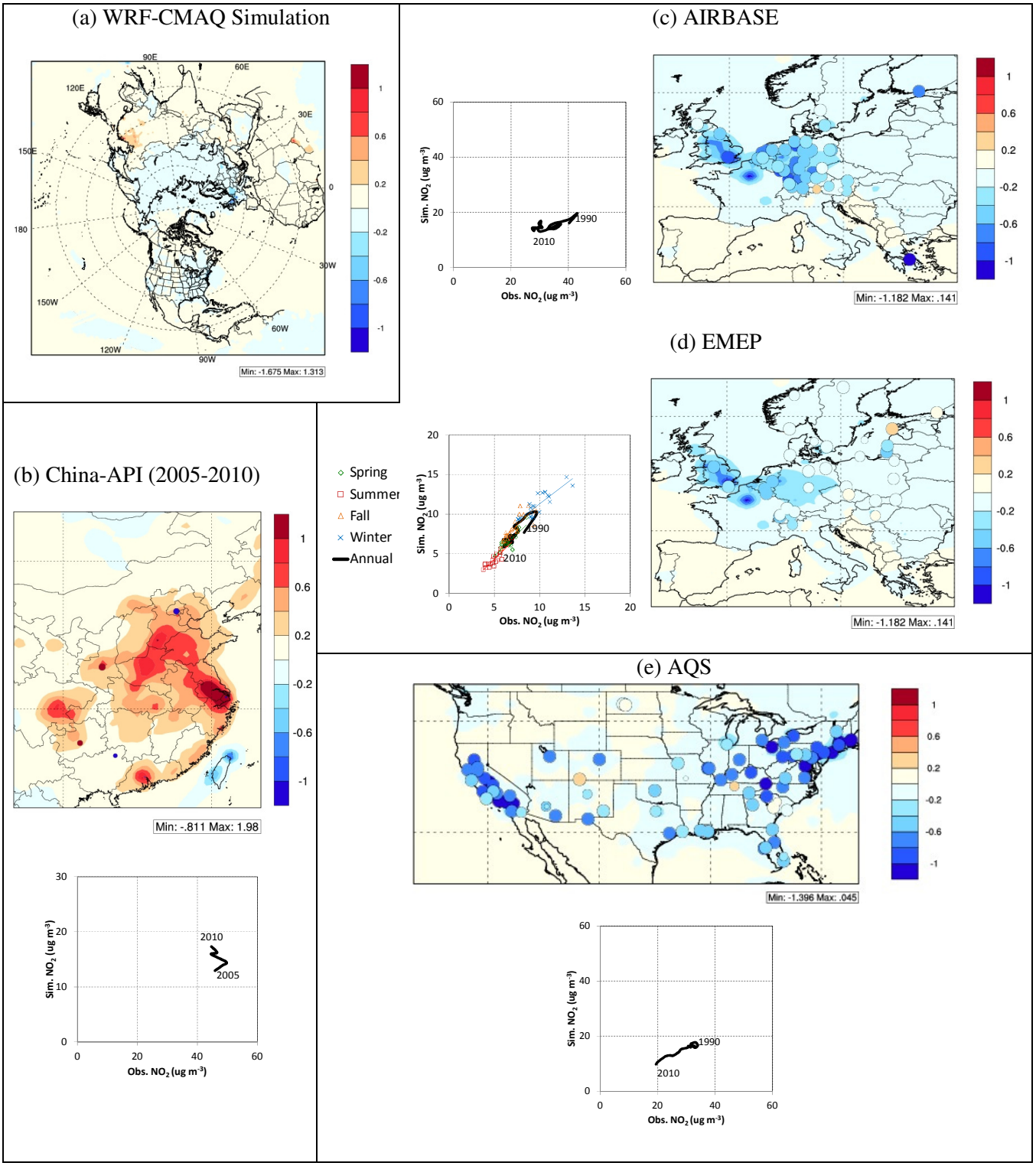

Fig. 4 Same as Fig. 3 for NO_2

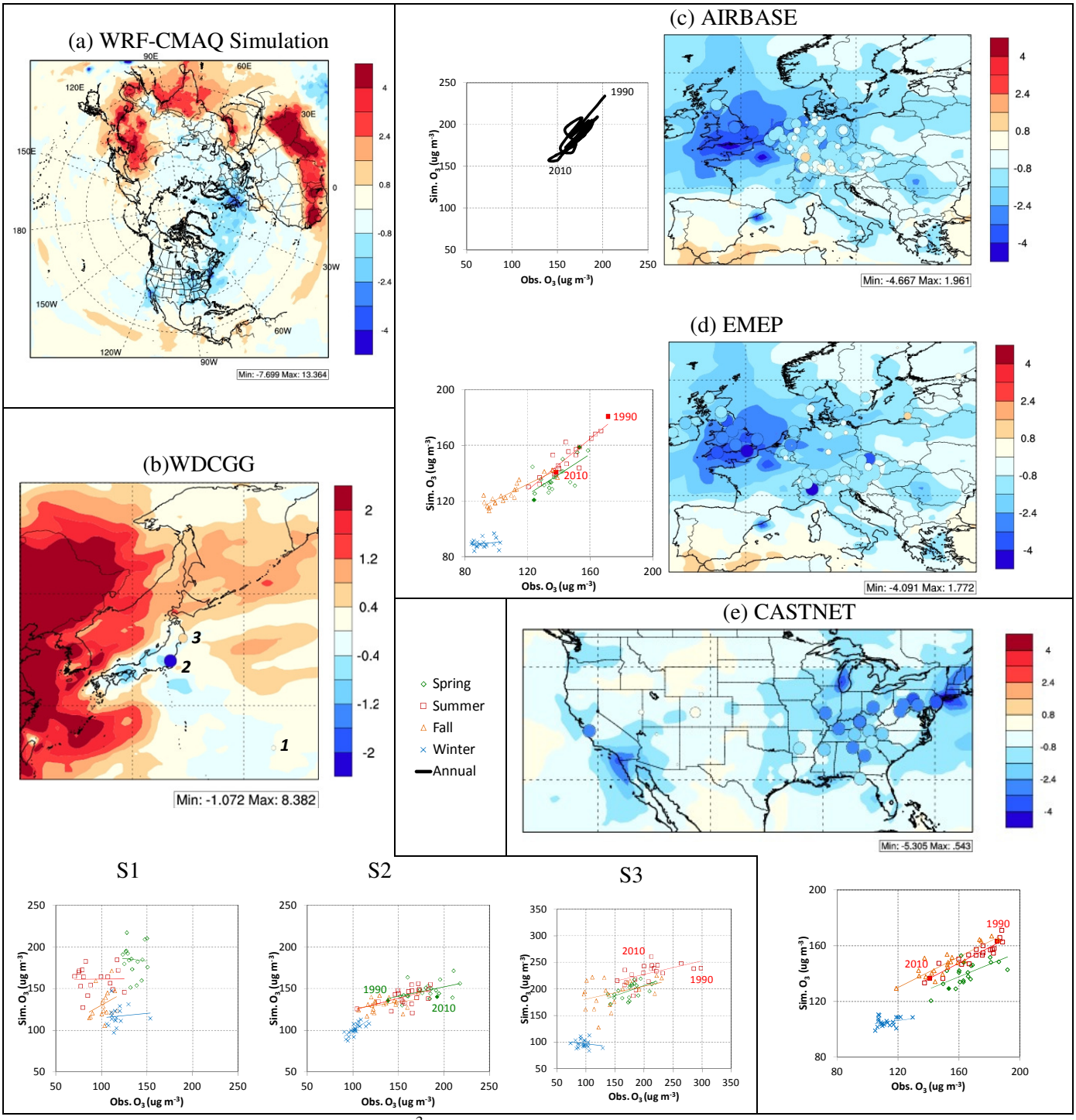

Fig. 5 Same as Fig. 3 for O_3 (unit: µg m^{-3}, computed on the basis of annual or seasonal maximum of DM8 (daily 8h maxima) value, except that for AIRBASE which is computed on the basis of annual maximum of DM1 (daily 1h maxima); three sites of WDCGG are S1- Minamitorishima, lat: 24.28, lon: 153.98, S2- Ryori, lat: 39.03, lon: 141.82, S3-Tsukuba, lat: 36.05, lon:140.13)

1

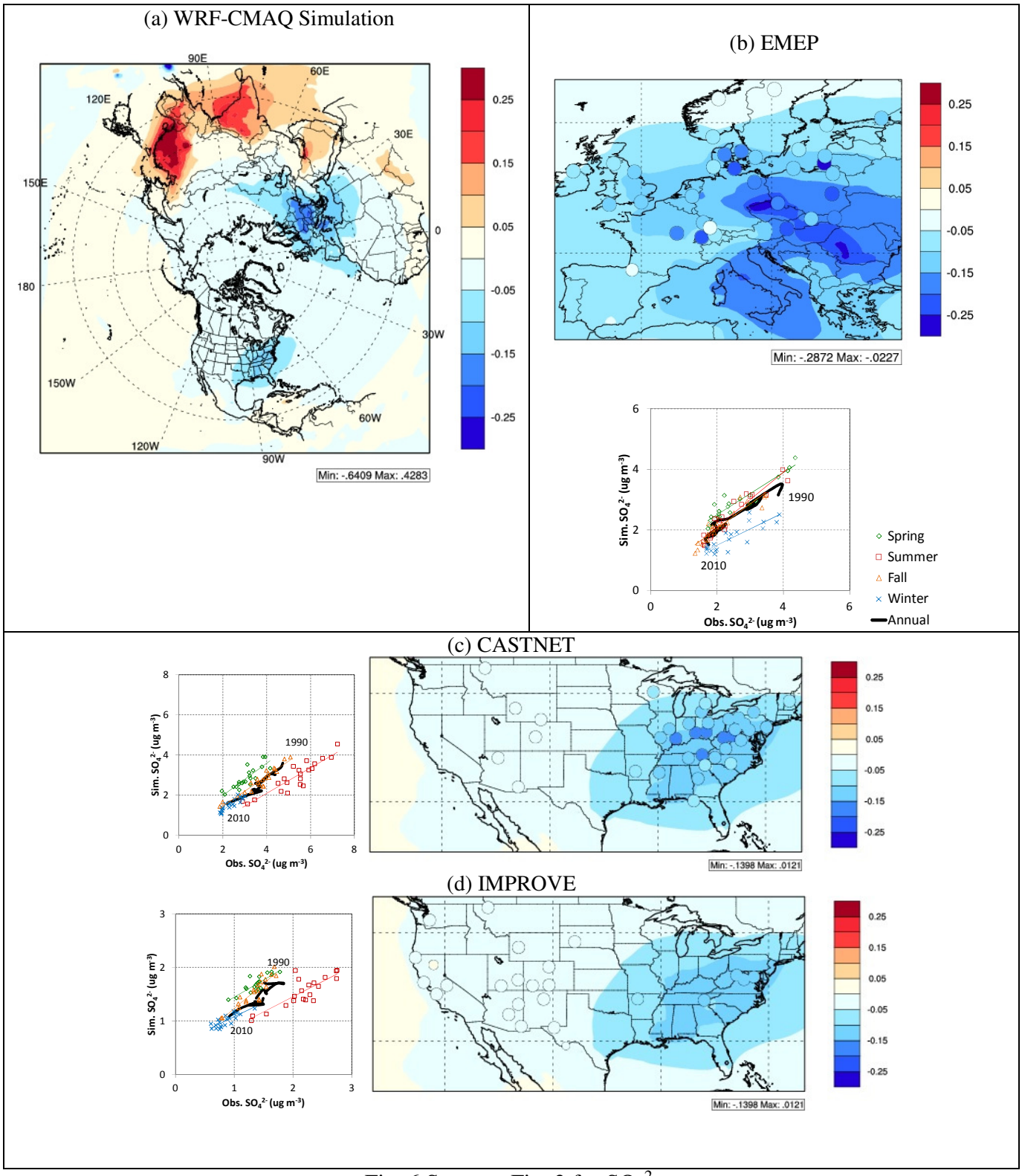

2 Fig. 6 Same as Fig. 3 for SO_4^{2-}

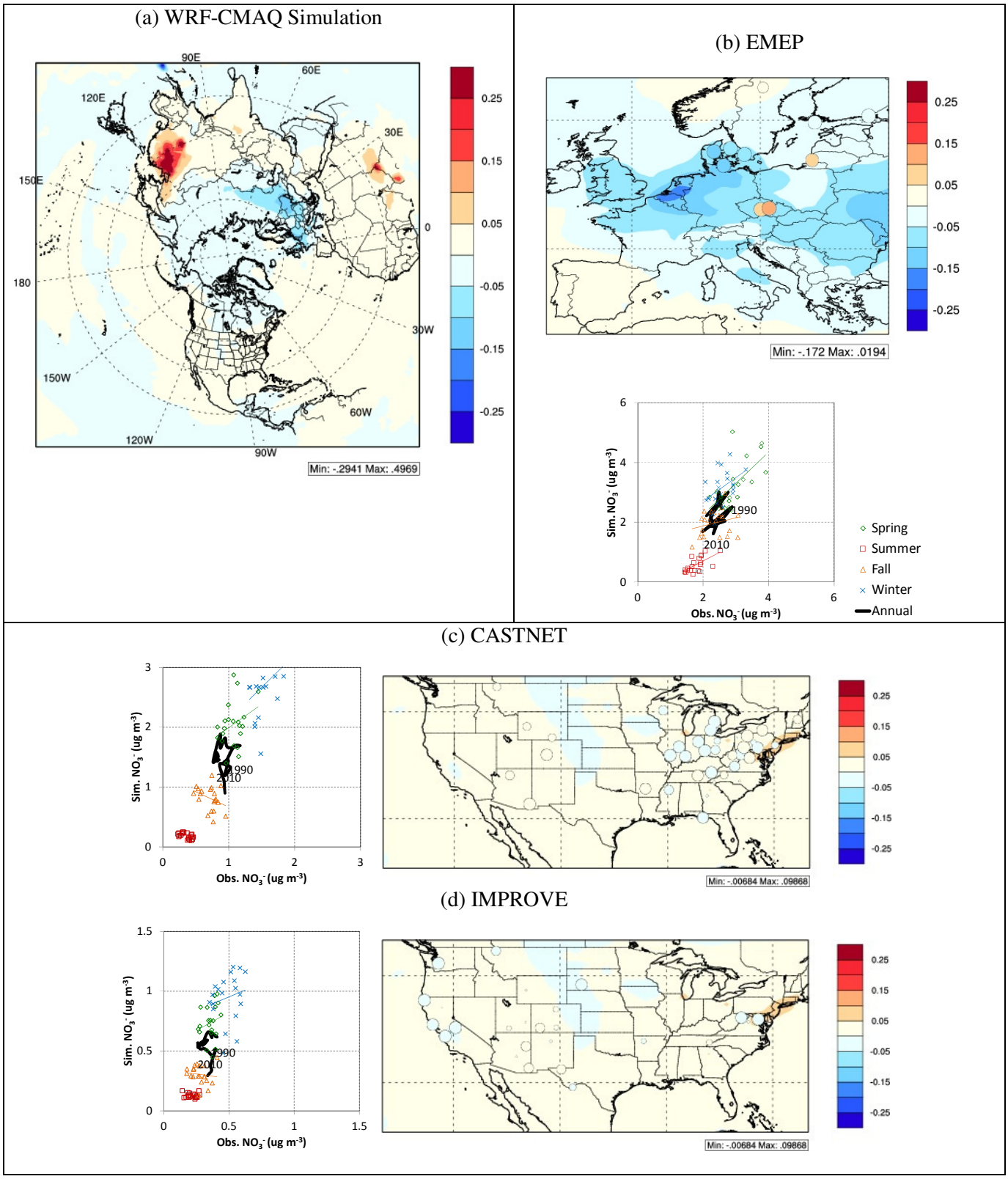

Fig. 7 Same as Fig. 3 for NO_3^-

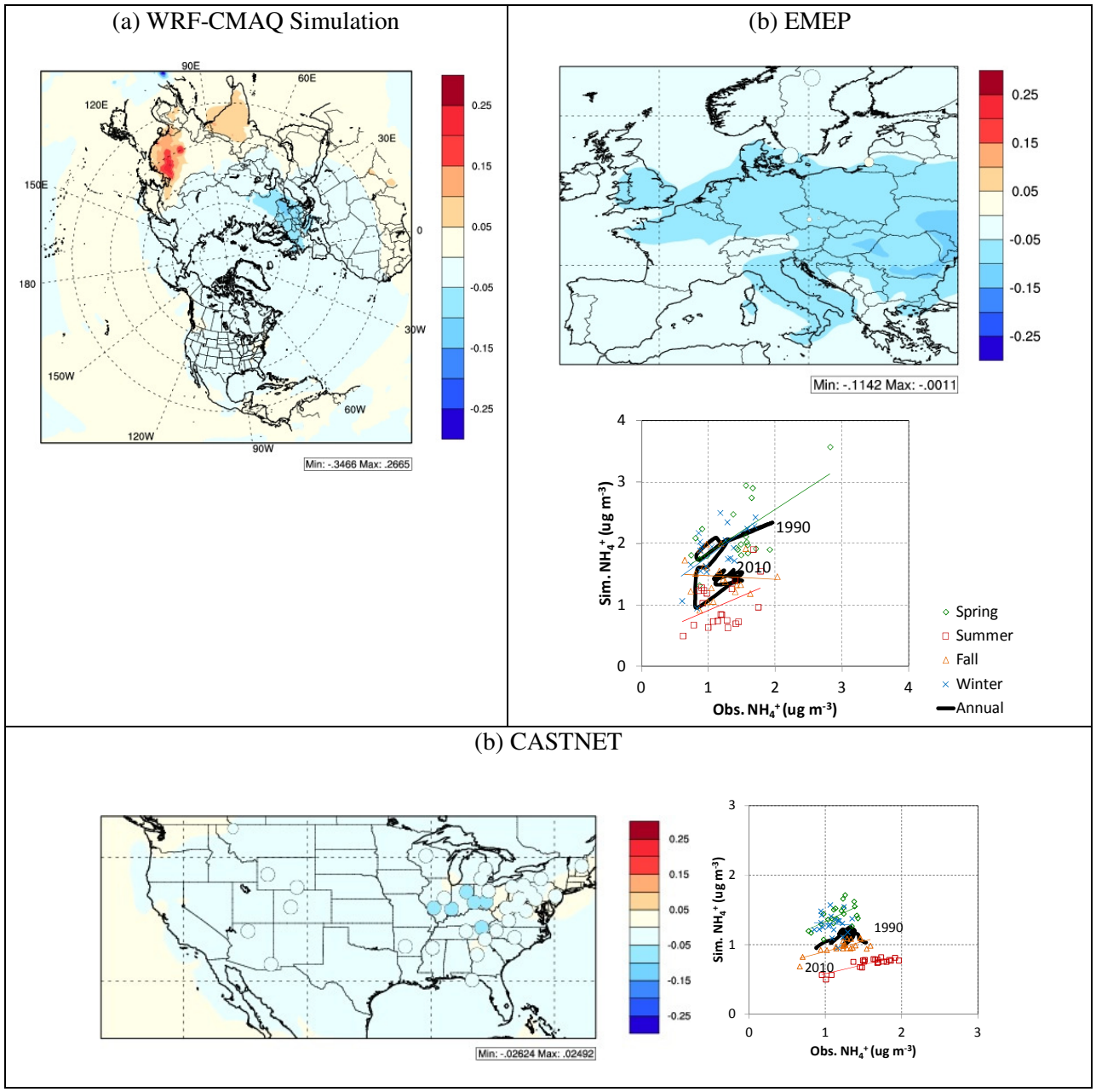

Fig. 8 Same as Fig. 3 for NH_4^+

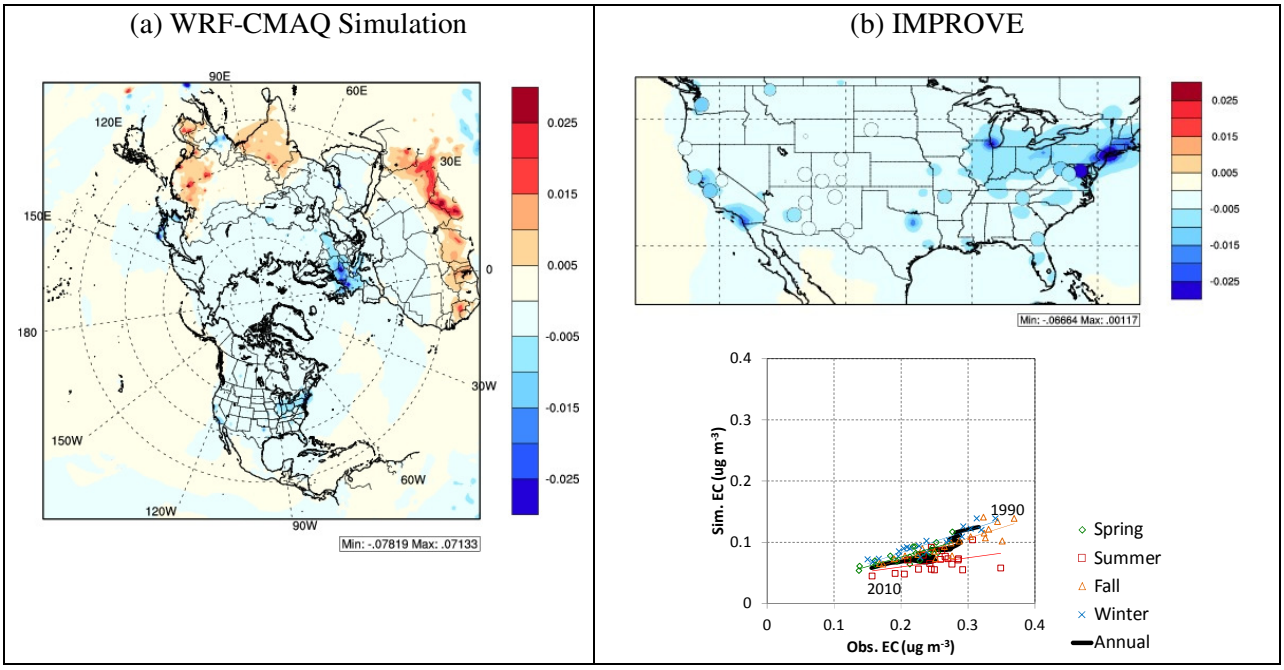

Fig. 9 Same as Fig. 3 for EC

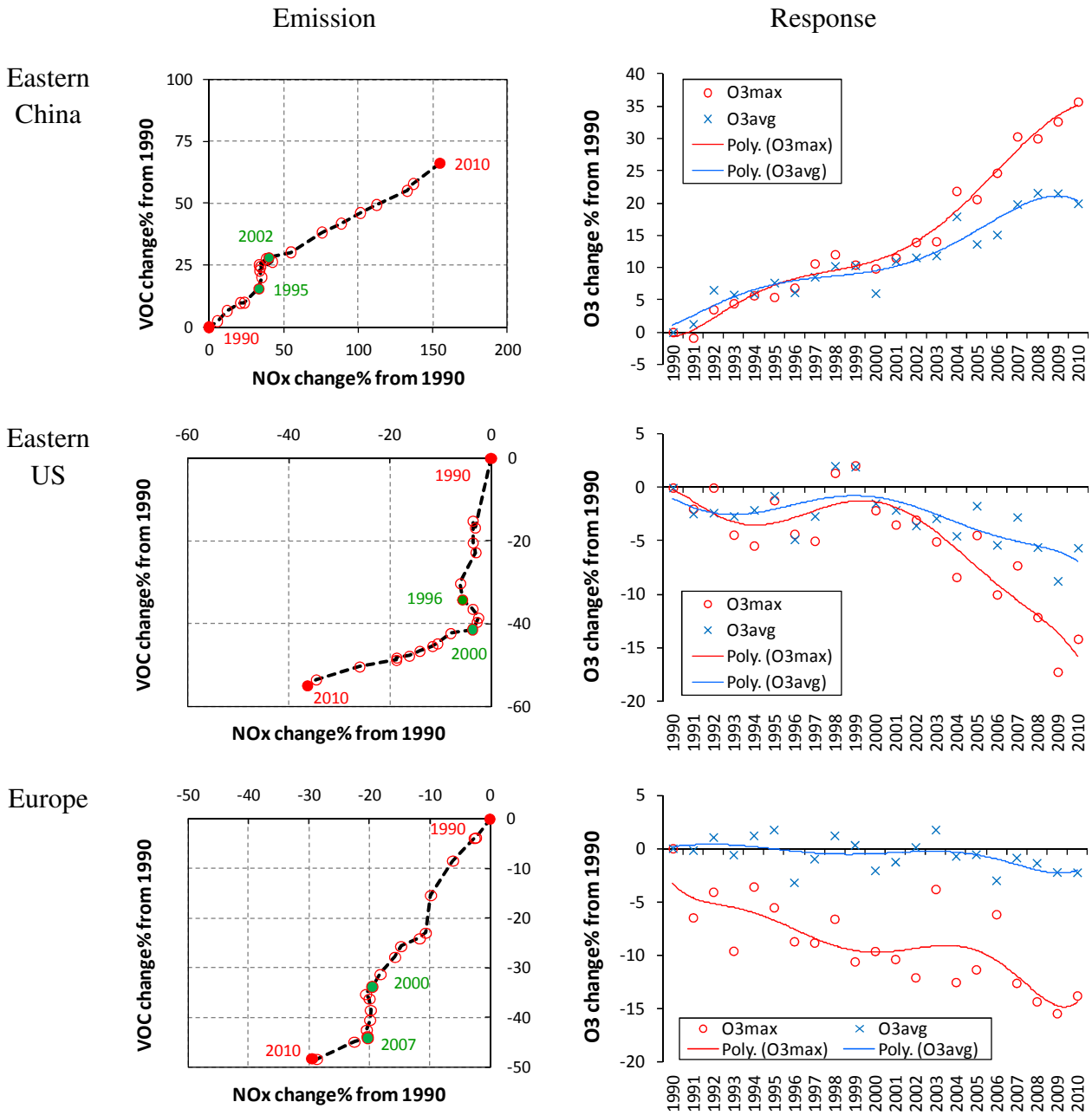

Fig. 10 Changes in O_3 chemistry from modeling results

(grid-averaged for three regions, O3max- maxima DM8 O_3 in each year; O3avg-avergaed DM8 O_3 in each year; Poly- trend fit by 6th order polynomial regression)

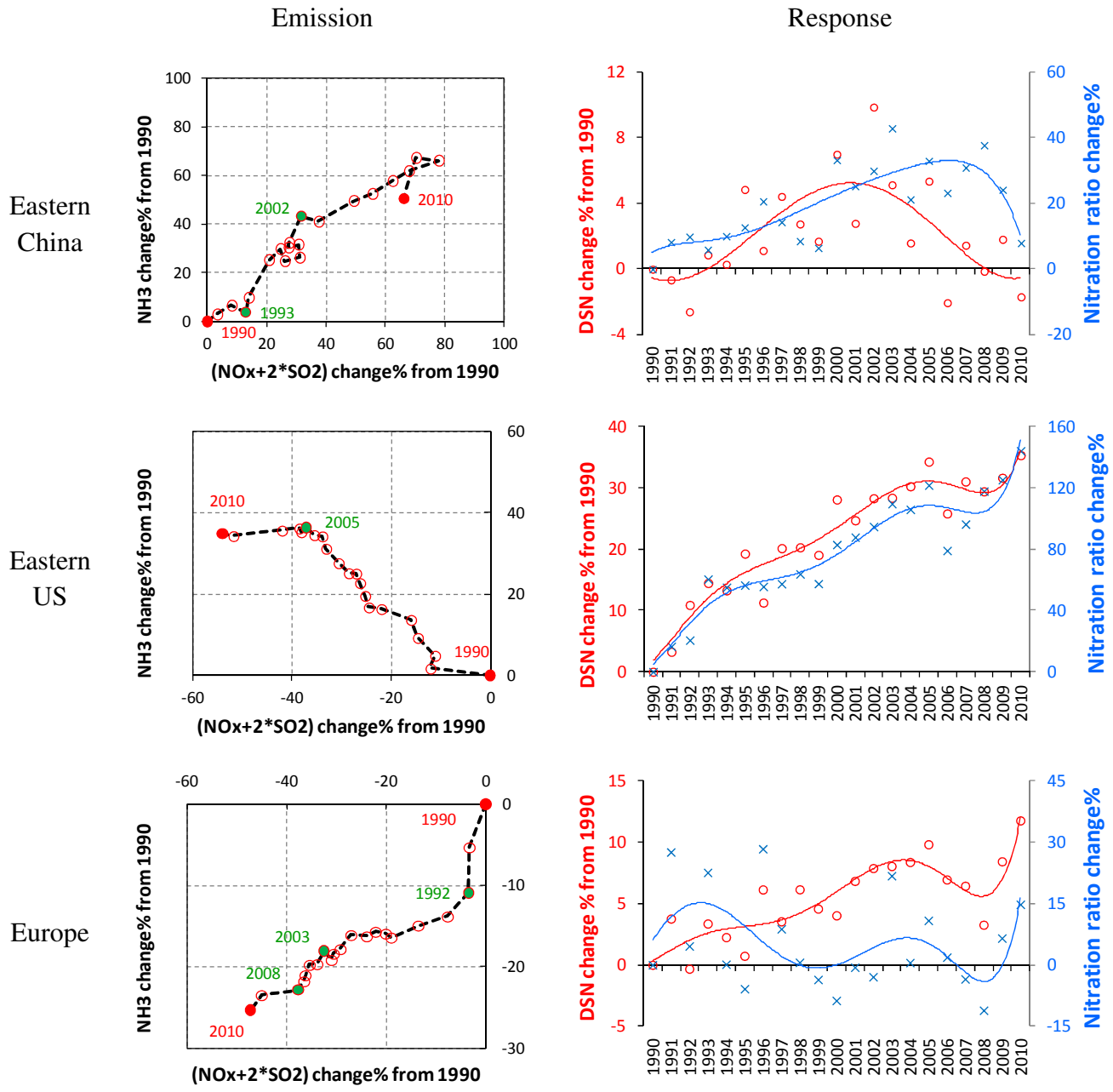

Fig. 11 Changes in PM chemistry from modeling results

(calculation based on molecular units; grid-averaged for three regions; (NO_x+2*SO_2) represents the amount of NH_3 needed for complete neutralization; DSN- degree of sulfate neutralization; Nitration ratio = NO_3^- concentration/NO_x emission)